Ca' Foscari
University
of Venice

Master's Degree in

Chemistry and Sustainable Technologies

Final Thesis

# Development of an electrochemical biosensing platform, based on bicyclic peptides as the synthetic receptors, to detect protein cancer biomarker h-uPA

**Supervisor**
Prof. Federico Polo

**Graduand**
Leonardo Ferrari
Matriculation Number 860685

**Academic year**
2021/2022

# Abstract

In recent years, developing devices aimed at detecting cancer biomarkers has become a critical need to face more demanding challenges in the field of healthcare. Human-urokinase plasminogen activator (h-uPA) has been recently recognized as a promising protein cancer biomarker gaining an increasing interest in the field of cancer research and sensing. In fact, novel methodologies and technologies, devised for cancer detection, are highly sought, particularly those employing synthetic receptors. In fact, the latter ones would enable providing an ease and economic way to develop a specific and sensitive recognition layer, while avoiding few of the drawbacks derived by the antibodies' production, as for example: (i) the use of animals, whose immune system is exploited to produce antibodies; (ii) the time required for the animal immune systems to produce the desired antibodies in large amount; (iii) the extraction, separation, and purification processes. A special class of bicyclic peptides, known to inhibit h-uPA, might have a central role in the recognition of this protein biomarker and in the development of specifically devised biosensing platforms, because they can act as synthetic receptors owing to their selectivity and high binding capacity. In this Thesis we propose the synthesis and characterization of a novel bicyclic peptide, whose performances toward h-uPA detection are tested upon developing an electrochemical biosensing platform. The results are then compared with those obtained with another peptide, which has been recently described in literature.

# Index

# 1. Introduction

## 1.1 Cancer

Cancer is a genetic disease that affects gene expression processes corrupting the DNA and inducing a mutations or epigenetic changes (not mutational) often caused by DNA methylation. The genes are involved in alterations of the normal cellular functions like growth, motility, and life cycle. The tumors are promoted by two classes of genes: oncogenes, the mutated ones, and tumor suppressor genes (TSGs), whose normal function is to inhibit cell cycle progression and apoptosis. However, if altered, they can bring to hereditary cancer diseases that will occur early in life. Eight main cancer hallmarks can be summarized as: (i) angiogenesis (the ability to create a blood supply for the tumoral cells), (ii) independence from growth factor, (iii) insensitivity to growth suppressors, (iv) avoidance of apoptosis (programmed cell death), (v) evading immune system, (vi) maintenance of replicative potential, (vii) modification of energy metabolism and (viii) invasion of other tissues (metastasis).[1]

In the last 50 years, cancer has become one of the biggest challenges in medical field, because of the difficulty in finding more and more efficient diagnostic methodologies and tools, and effective therapies. In 2020 there were estimated 19.3 million cases and 10 million deaths worldwide distributed in 36 cancer types. Among which, the most common ones are targeting female breast, lung, prostate, nonmelanoma of skin and colorectal, as shown in **Figure 1**.[2] In the USA it is also the second main cause of deaths, overcome only by hearth diseases, with 599.601 cases on the total number of 2.854.838 in 2019 and a mortality incidence of 21%. The projection for 2040 shows an increase of both the cases and the deaths to 4.75 and 2.55 million, respectively, owing to the ageing and growth in population number.[3]

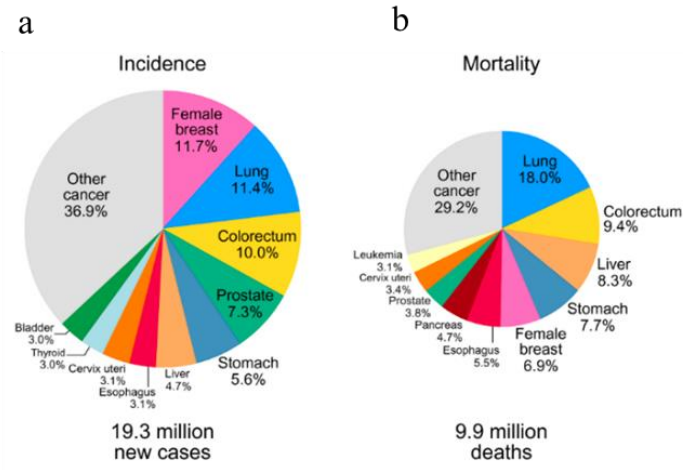


**Figure 1.** Distribution of (a) cases and (b) deaths for the 10 most common cancers in year 2020 for both sexes.[2]

Despite these data are not encouraging, as shown in **Figure 2,** many studies directed toward prostate (male) and breast (female) cancers showed that their incidence rate has decreased since 1990, also thanks to the discovery of new screening methods. In fact, novel diagnostic tools allowed to early diagnose prostate cancer patients, thus improving their survival perspectives. Similar conclusions hold for the incidence rate of breast cancer, which decreased of 42 %.[4]

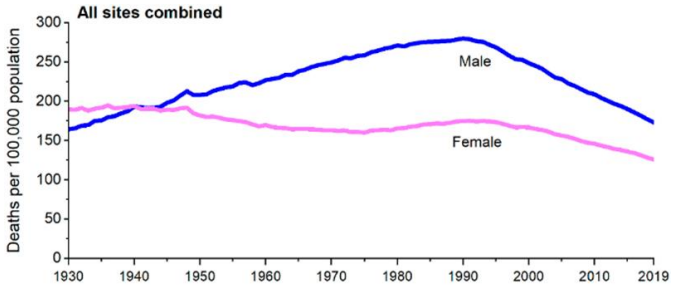


**Figure 2.** Incidence rate for male and females per 100.000 people for all cancer types since 1930 to 2019.[4]

Nowadays the screening process is fundamental for the prevention and early detection of the disease in patients without symptoms, but also to improve the effect of prognosis.[3] The World Health Organization (WHO) provides the guidelines for the screening tests and the requirements they have to fulfill: (i) sensitivity, (ii) effectiveness to detect the disease in true patients, (iii) specificity and (iv) reliability of positive and negative results.[5]

## 1.2 Urokinase-type Plasminogen Activator

### 1.2.1 uPA-uPAR system

Urokinase Plasminogen Activator (uPA) is a serine protease, component of the urokinase plasminogen activator system and has important functions in tissue remodeling and cell migration.[6] As summarized in **Figure 3**, this system regulates the transformation of plasminogen, a single chain polypeptide, into plasmin, a protease involved in cancer invasion and metastasis by the degradation of extracellular matrix (ECM) proteins, such as: fibronectin (FN), vitronectin (VN), fibrin, laminin and osteopontin. It is also involved in the activation of certain growth factors, which can lead to proliferation and migration, and specific metalloproteases, which degrade some forms of collagens.[7,8]

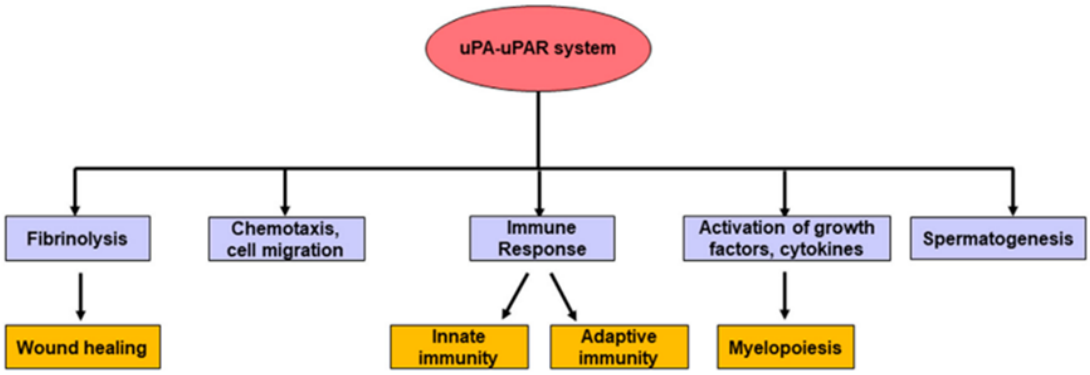


**Figure 3.** The principal physiological regulating functions of the urokinase plasminogen activator system. [9]

The human uPA (h-uPA) protein (50 kDa) structure consists in two polypeptide chains bonded to each other with disulfide bridges. The A chain has two domains, the growth factor domain (GFD) and a kringle domain, while the B chain has the catalytic domain.[10]

In **Figure 4** the interaction between the amino-terminal fragment of uPA and the three domains of uPAR is depicted.

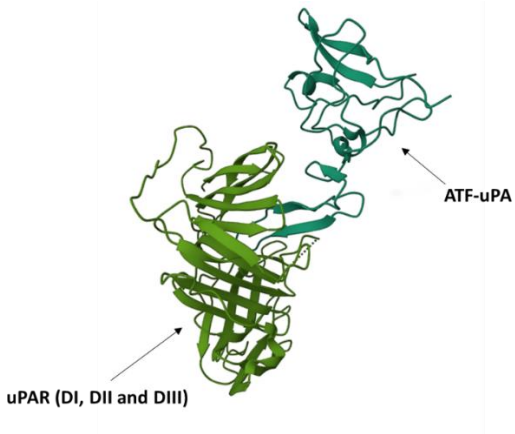


**Figure 4.** Crystal structures of amino-terminal fragment (ATF) of urokinase-type plasminogen activator (uPA) (dark green) linked to the three domains (DI, DII and DIII) of its receptor uPAR (PDB ID: 2I9B).[11]

## 1.2.2 uPA as cancer biomarker

In recent years, the interest toward uPA as prognostic or diagnostic biomarker, as well as therapeutic drug, has gained attention.[6] Concerning the prognosis, its presence can be related to several types of cancer, such as breast, prostate, colorectal and lung. Since decades many studies reported the strict correlation between uPA protein and breast cancer occurance.[12, 13] Its antigen levels in normal breast tissue was verified to be at 0.11 ng per mg of proteins, while in breast cancer tissue at 0.88 ng per mg of proteins, proving a great increase in uPA levels in the latter case.[14] In other two case studies, the range of levels in tumoral tissues were found between 0.22-21.8 ng per mg of proteins and < 24.95 ng per mg of proteins.[15, 16] Its serum levels were measured in 252 positive patients obtaining a median value concentration of 2.52 ng $mL^{-1}$ and a range between 0.21-16.06 ng $mL^{-1}$.[17]

In breast cancer detection uPA has been proven to be a better prognostic marker than others well-known, such as estrogen receptor, progesterone receptor, epidermal growth factor receptor (EGFR) and human epidermal growth factor receptor 2(HER2).[18]

An example of application of uPA in a breast cancer detection device is an ELISA kit, FEMTELLE®, commercially available and validated by an external quality assessment (EQA) program and the American Society of Clinical Oncology (ASCO). In **Figure 5** two possible diagnostic pathways for breast cancer involving uPA as biomarker are shown.[9]

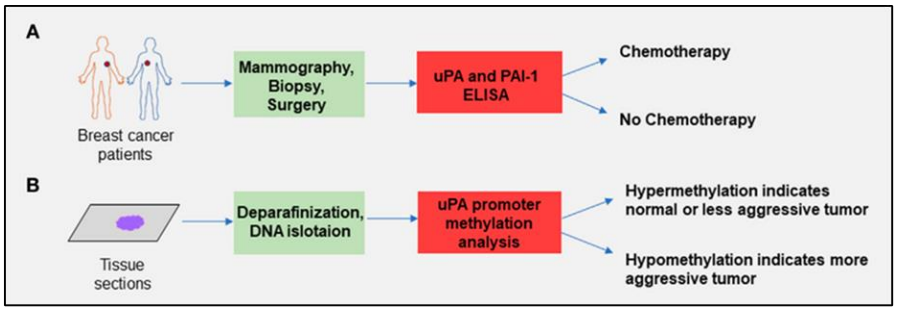


**Figure 5.** Two promising diagnostic methods for breast cancer detection with uPA.[9]

## 1.3 Biosensors in cancer diagnosis

### 1.3.1 What is a biosensor?

Biosensors are normally defined as chemical sensor that uses a biochemical mechanism as the recognition system of the analyte.[19, 20] IUPAC defines chemical sensors as devices that produce analytical signals from chemical information, like concentration, and they consist of two main components: the chemical recognition system (receptors) and a physicochemical transducer. In biosensors the first has the task of recognizing biological receptors through biochemical data and to translate that into chemical or physical output, as illustrated in **Figure 6**.

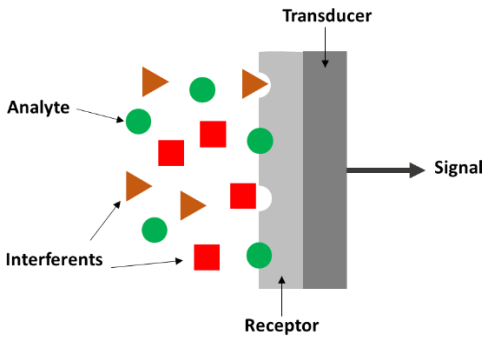


**Figure 6.** Schematic representation of the basic function of a biosensor, in which the receptor sites recognize the analyte and the transducer translates the chemical output into an electric signal.

The two most important characteristics are sensitivity, the ability to recognize the lowest value of (bio-)chemical information possible, and selectivity, the capacity to detect selectively only the desired (bio-)molecules.[21] The analytes can be regarded as: ions, dissolved gases, vapors, substrates, antibodies/antigens, proteins and LMW (low molecular weight) substrates.[22]

Generally, biosensors are developed by employing biomolecules as the receptor for the analyte of interest. In electrochemical biosensor the receptor is usually bound or in close proximity to the electrode surface to form the molecular recognition layer.

The types of receptors that are employed can be summarized as follows:

1- Antibodies, immune system proteins featuring high specificity and affinity.
2- Lectins, non-immune proteins with great affinity with glycoproteins and glycolipids.
3- DNA (deoxyribonucleic acid), an excellent receptor owing to its stability and molecular adaptability.
4- PNAs (peptide nucleic acids), non-natural nucleic acids that offer enhanced chemical and thermal stability than DNAs and RNAs.
5- Aptamers, single-stranded DNA or RNA sequences capable of generating 3D structures when they bind to analytes.
6- MIPs (molecularly imprinted polymers), featuring an ease preparation by deposition on electrodes.
7- Peptides, short amino acid chains (20-30 units) that offer chemical stability, ease synthetic procedure (often automated) and show good selectivity to many cancer biomarkers.[23]

The function of the transducer is to translate the recognition event into an electric output. If this is based on an electrochemical technique, the biosensor is defined electrochemical. Some examples of transducers for electrochemical devices are: ion-selective (ISE), glass, gas and metal electrodes for analytes like ions ($K^+$, $Cl^-$, $Ca^{2+}$, $F^-$, $H^+$, $Na^+$...), $CO_2$, $NH_3$ and redox species, metal, carbon and chemically modified (CME) electrodes for molecular oxygen, alcohols, sugars, phenols and oligonucleotides, interdigitated and metal electrodes to detect urea, oligonucleotides and charged species, ion-sensitive field effect transistors (ISFET) and enzymes FET (ENFET) to analyze cations like $H^+$.[21, 22] The applications of electrochemical biosensors can be found in many different fields like food industry and medicine with good results and perspectives, as the increasing number of research studies about this topic and reported in **Figure 7** demonstrates:

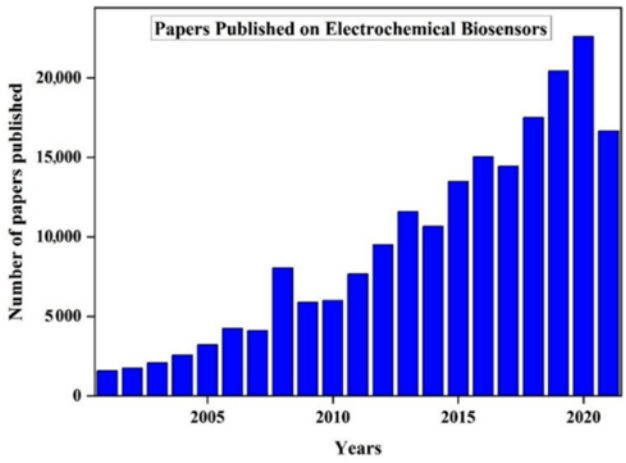


**Figure 7.** Reviews and articles published from 2000 to 2021 about electrochemical biosensors.[24]

Undoubtedly, the most important application field of electrochemical biosensors is related to the healthcare. In many medical procedures biosensors obtained an important role: detection of biological abnormalities, heart rate and rhythm monitoring in patients with cardiac illnesses, studies of air quality for healthcare purposes, management of disease, monitoring of post-surgery treatments and detection and quantification of biomolecules, as illustrated in **Figure 8**.[25]

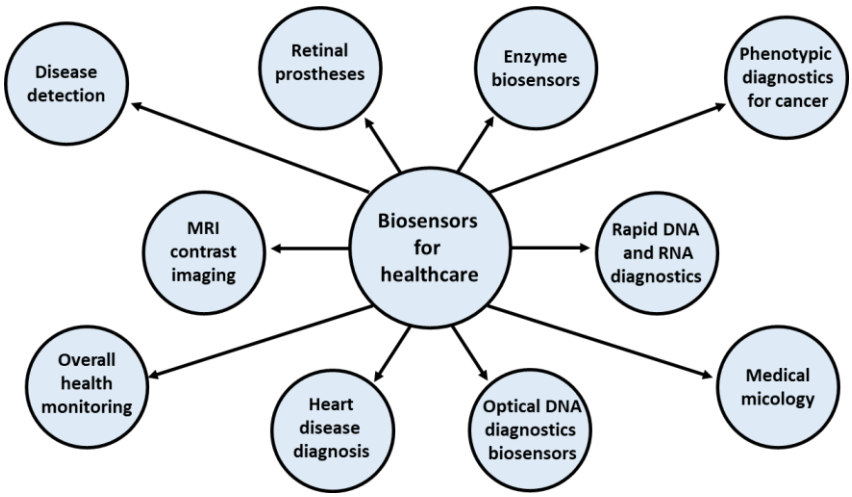


**Figure 8.** Most common applications of biosensors in healthcare service.[25]

Electrochemical biosensors aimed at cancer diagnosis show a huge potential, owing to their ease of fabrication and low production costs, high sensitivity and reproducibility, robustness, and miniaturization. They can be easily integrated within microfluidic systems to offer a plethora of devices, whose working principle can benefit of different methodologies, such as: conductimetry, potentiometry, amperometry, voltammetry, impedance spectroscopy and field-effect.[26, 27]

## 1.4 Electrochemical techniques

Electrochemistry is the branch of chemistry that studies the chemical transformations initiated by electrical processes and, vice versa, the production of electric current by chemical reactions. In the latter case, there are involved the processes and factors affecting the electron transfer (eT) across interfaces between an electrode (an electronic conductor) and an electrolyte solution (ionic conductor) where the analyte of interest or an electroactive specie (that can undergo oxidation or reduction) is dissolved and freely diffuses in.

An electrochemical cell is composed by a working electrode (WE), where the above-mentioned eT process is occurring, a counter electrode (CE), and a reference electrode (RE), which serves to precisely control the potential (energy) applied to the system to make the electrochemical reactions (oxidation and reduction) occur.[28]

Voltametric methods pertain the application of a potential, which varies with time according to a specific function, to the WE, thus causing the oxidation or reduction (redox processes) of an electrochemically electroactive specie at the electrode surface. From the electrochemical pattern, one can obtain insights about the redox processes, the nature of the analyte and its concentration. Among the most widely used electrochemical techniques there are the voltametric and impedance techniques. For the aim of this Thesis work, herein we will deal mainly with differential pulse voltammetry (DPV) and electrochemical impedance spectroscopy (EIS), which will be briefly discussed in the following sections.

### 1.4.1 Differential Pulse Voltammetry (DPV)

This method consists in small voltage pulses of a certain amplitude superimposed 3-5 times per second on a linear voltage ramp (see **Figure 9**). The currents are recorded as differences between the current at the end of the pulse and the one at the beginning of it. The current difference is then plot against the applied potential, thus obtaining the voltammogram. This process prevents the overlap of different peaks related to different compounds and allows to obtain sharp peaks, increasing the resolution over traditional voltammetric measurement (e.g. cyclic voltammetry).[29]

The height of each detected peak is directly proportional to the analyte concentration in the sample according to the following relation (eq.1):

$$i_p = \frac{nFAD^{1/2}C}{\sqrt{\pi t_m}}\left(\frac{1-\sigma}{1+\sigma}\right) \qquad \text{(eq.1)}$$

Where $\sigma = e^{\left[\left(\frac{nF}{RT}\right)\left(\frac{\Delta E}{2}\right)\right]}$ and ΔE is the pulse amplitude. The quotient $\left(\frac{1-\sigma}{1+\sigma}\right)$ reaches the maximum value (unity) with large amplitudes. Moreover, this technique makes a significant correction to the charging current due to the background contribution (solvent/electrolyte), allowing to measure concentrations around $10^{-8}$ M.[30]

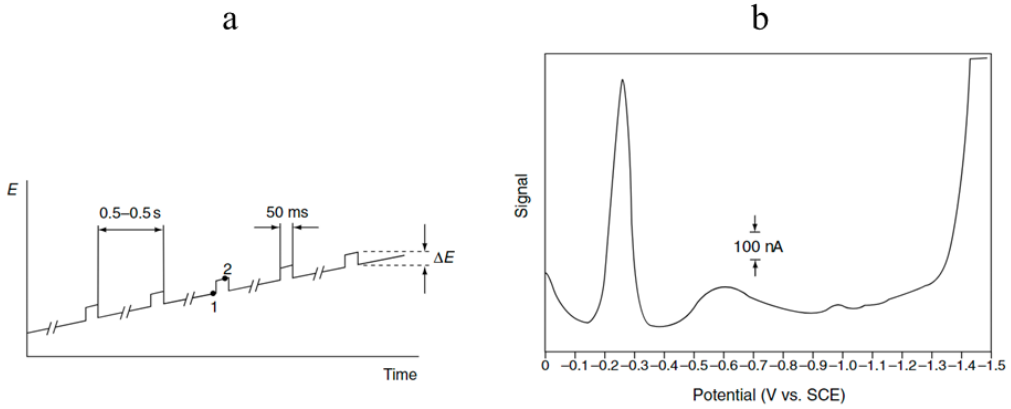


**Figure 9.** (a) Potential vs time plot that shows the evolution of potential in time. The points where the current difference is sampled are shown: before the pulse start (**1**) and at the pulse end (**2**). (b) Typical voltammogram (I vs E) of a DPV measurement.[30]

## 1.4.2 Electrochemical impedance spectroscopy (EIS)

When an alternate current (AC) sinusoidal potential, expressed as $E_{ac0}\sin(\omega t)$, is applied to a resistance (R) generates another sinusoidal current ($I_{ac0}\sin(\omega t)$). Since the relation that links these three physical quantities is the following (eq. 2):

$$R\ (\Omega) = \frac{E\ (V)}{I\ (A)} \qquad \text{(eq. 2)}$$

It is clear that R is independent from the phase ωt, and also from the frequency of the applied wave (ω=2πν). Therefore, it can be rewritten as (eq. 3):

$$R\ (\Omega) = \frac{Eac0\ (V)}{Iac0\ (A)} \qquad \text{(eq.3)}$$

where $E_{ac0}$ is the potential amplitude and $I_{ac0}$ is the current amplitude.

However, in an electrical circuit, besides the resistor, one has to consider also other two components: the capacitor and the inductor, whose resistances are dependent on the phase. Having a magnitude and a phase, this kind of resistance, i.e. the impedance, can be expressed as a complex number in polar coordinates or in Cartesian coordinates having a real and an imaginary part.[31]

The EIS adopts these concepts and applies them to an electrochemical system within an electrochemical cell (usually a three-electrodes cell). In particular EIS investigates the interactions between electrolyte, electroactive species and electrode in terms of charge-transfer, mass-transfer from bulk solution to electrode surface, resistance of the electrolyte and concentrations of species. These phenomena can be regarded as an electrical circuit with resistors, capacitors, inductors and constant phase elements connected in series or in parallel.

The type of electrical circuit to choose depends on the interface electrolyte/electrode. The EIS plot is mainly represented in two ways: if the imaginary part of impedance ($Z_{imag}$) is plotted versus its real part ($Z_{real}$), the Nyquist plot is obtained (see **Figure 10**). Whereas the Bode plot consists of two separate plots in logarithmic scale, one concerning the magnitude vs. phase, the other the phase vs. frequency.[32]

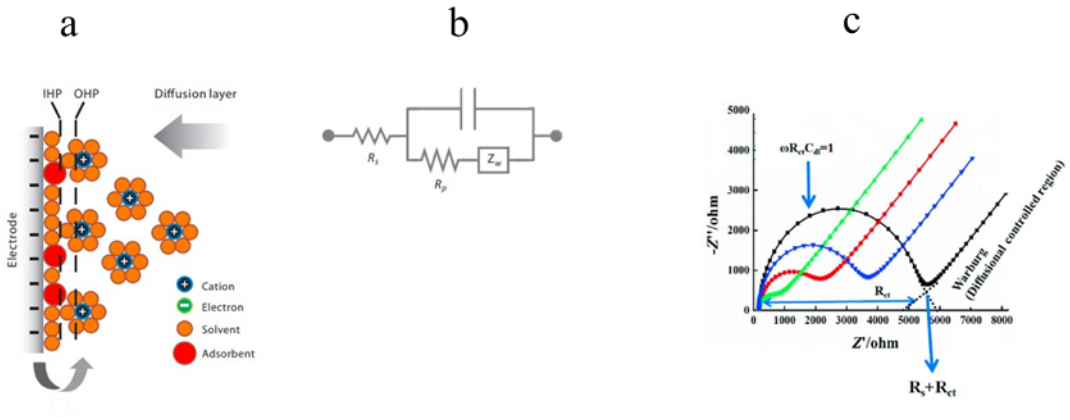


**Figure 10.** (a) Schematic representation of an ideal interface electrode (negatively charged)/electrolyte solution, (b) the circuit that represents it, called Randles equivalent circuit, and (c) an example of a Nyquist plot related to it. The Randles EC principal components are the resistance of the bulk solution ($R_s$), the double layer capacitance ($C_{dl}$), the polarization (or charge transfer at the standard electrode potential) resistance ($R_p$ or $R_{ct}$), the Warburg resistance ($Z_w$ or W) and in some cases an additional one is the constant phase element (CPE) that mimic the non-ideal capacitance behavior.[32, 33]

## 1.4.3 Screen-printed electrodes (SPE)

In recent years screen-printed electrodes (SPE) became very important in the development of modern electrochemical sensors with high performances. They offer several advantages, which are mainly related to the miniaturization of the devices that allows to analyze smaller sample volumes of the order of microliters. Furthermore, the versatility of the electrode materials used, which can be modified according to the required application and to a specific analyte. Their implementation and integration in many different portable devices to allow in situ measurements. In addition, the possibility of a rapid mass-scale production helped to remarkably lower the production costs.[34] SPE are produced through screen-printing technique, similar to 3D, where every layer is deposited and then hardened. The supporting material can be plastic, organic polymers, ceramic, alumina, glass, nylon and others, whereas the printed materials initially are deposited as inks, such as carbon (graphene, graphite, fullerene and carbon nanotubes) silver, gold and platinum.[35] Nowadays SPE fabrication is based also on the use of renewable and biocompatible sources or waste materials like paper, agricultural byproducts, CD or DVD and batteries, favoring the reductions of costs and the recycle of materials.[36] The screen-printing method allows also to create many different shapes with different purposes, such as discs, rings and bands. The electrode surfaces can be also modified with other materials, like nanoparticles, and substrates such as polymers, Schiff bases and biomolecules (antibodies, enzymes and nucleid acids).[35] **Figure 11** shows an example of the SPE used in this Thesis work [37] and the well-known and worldwide employed glucose sensor featuring an SPE integrated with lateral flow technology.[38]

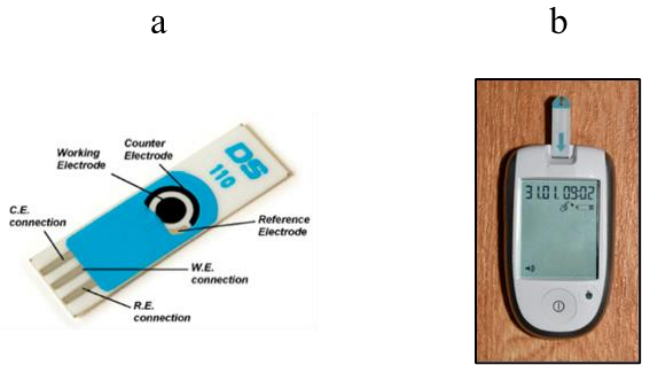


**Figure 11.** (a) Main components of an SPE and (b) a commercially available glucose sensor.[37, 38]

## 1.5 Peptides

Peptides are natural or synthetic molecules that consist of aminoacidic units (up to 100) connected to each other via amide (peptide) bonds, as shown in **Figure 12**. They can be differentiated in two classes according to IUPAC: oligopeptides, which have from 10 to 20 aminoacidic residues, and polypeptides, that have from 20 to 100 monomer units and are the basic component of proteins.[39, 40] With all the possible combinations of the 20 natural amino acids, the number of different peptides that can be synthetized is countless. The R-group linked to the alpha-carbon ($C^{\alpha}$) of each aminoacidic monomer can provide the peptide with peculiar chemical properties depending on its nature.[39]

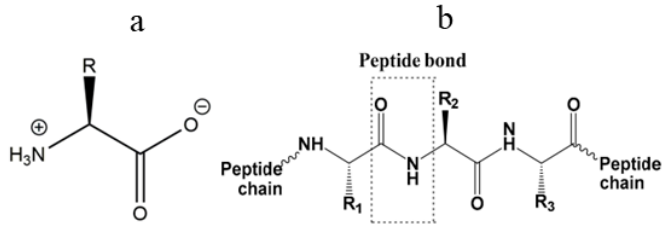


**Figure 12.** (a) Basic structures of an amino acid and (b) a peptide chain highlighting the peptide, or amide, bond.[41]

The applications of synthetic and natural peptides in medical field are several: as antimicrobial and anticancer molecules[42], in vaccines, as radio-theranostic agents, as protein mimetics, as drug delivery system (CPPs), in targeting cancer.[43]In electrochemical biosensors peptides can be used as cleavage sites for proteases, as phosphorylation sites for kinases, as antifouling agents, in self-assembled monolayers (SAMs) and as bioreceptors (see **Figure 13**).[44]

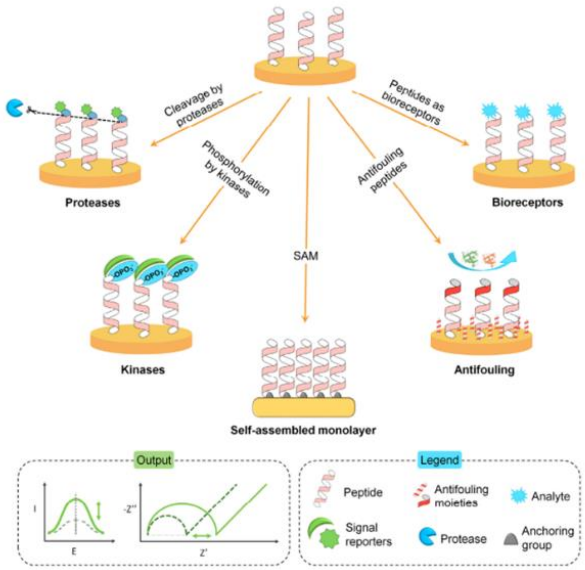


**Figure 13.** Scheme of the principal roles of peptides in electrochemical biosensors and the two types of output that can be obtained: signal "on", increasing, and signal "off", decreasing.[44]

Peptides also became an important alternative to antibodies as bioreceptors in immunosensors with many advantages depending on their stability, ease of synthesis and in engineering the structure and the reduced dimensions. These properties decrease steric hindrance and increase the sensitivity of devices and make them adaptable to many types of bio- and non-bio molecules like: metallic ions (heavy metals, such as lead, mercury and cadmium), DNA, peptides, cells and proteins.[45]

The application of peptides as bioreceptors in detection of target proteins and antibodies is well-known and there are a broad number of devices that can be used in clinical diagnosis and medical survey[45], like in the detection of biomarkers for HIV[46], Alzheimer's disease[47] and for different types of carcinoma [48, 49], including breast cancer.[50] An example of a peptide-based electrochemical biosensor for a tumoral marker is depicted in **Figure 14**.

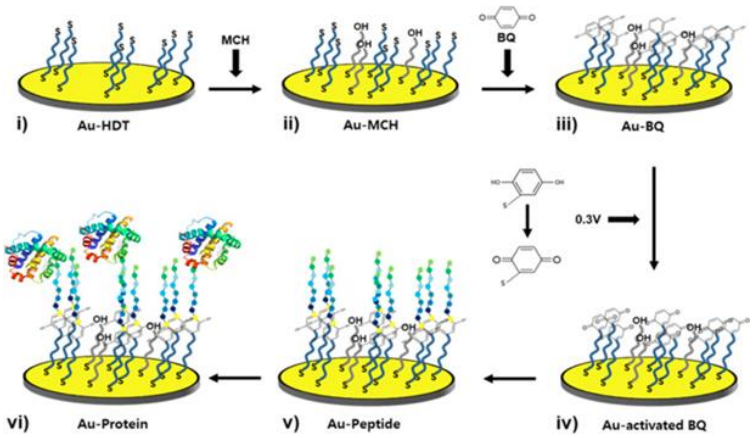


**Figure 14.** Scheme of the assembling procedure of an electrochemical biosensor for leucine-rich α-2-glycoprotein-1 (LRG1), a biomarker for colorectal cancer, with a peptide as bioreceptor. The gold electrode surface is functionalized with 1,6-hexanedithiol (HDT), 6-mercaptohexanol (MCH) and then benzoquinone (BQ). The surface is activated via electrochemical oxidation and then the peptide bioreceptor is added and subsequently the protein, that is detected with SWV (Square Wave Voltammetry) measurement.[49]

Linear peptides lack of a defined structure, because of their difficulty in make intramolecular interactions. Conversely proteins have tertiary and quaternary structures that confer thermodynamic stability and efficiency in their biological functions. Then using conformational constraints to reduce the structural freedom allows to improve those two properties.[51] To obtain a cyclic or multicyclic peptide, the possible synthetic strategies are: the chemical ligation and bridging of the peptide with side-chains or terminal groups that can induce the cyclisation process; the chemical ligation of peptides onto scaffolds like bis-, tris-, and tetrakis (bromomethyl) benzene derivatives[52], called CLIPS, or the chemo-enzymatic peptide synthesis (CEPS)[53].

Other relevant classes of constrained peptides are stapled peptides, which have an α-helical structures stabilized by "staples" molecules[54] and β-hairpin peptides[55]. The three previously described constrained peptide types are shown in **Figure 15**.

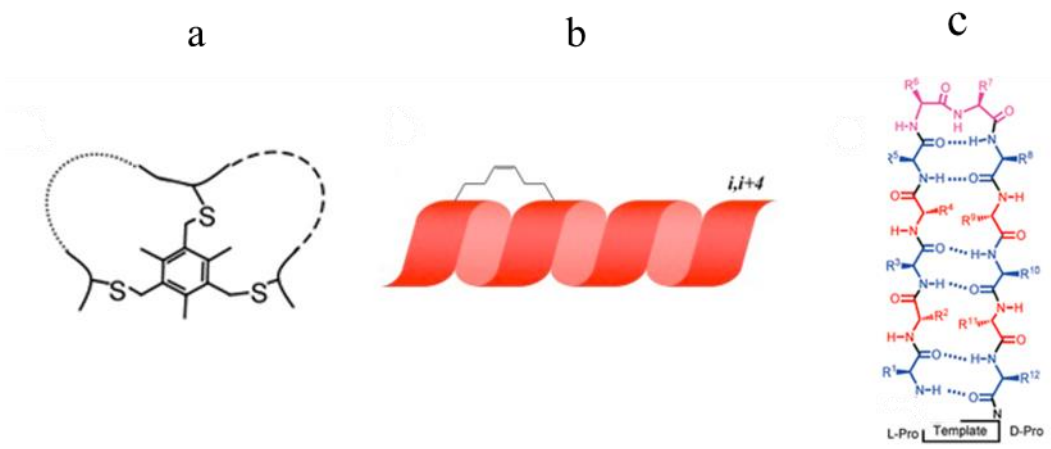


**Figure 15.** Three principal structures of constrained peptides: (a) multicyclic[52], (b) stapled[54] and (c) β-hairpin[55].

## 1.5.1 Bicyclic peptide's role in cancer diagnosis

Bicyclic peptides, having greater conformational rigidity and metabolic stability than linear and monocyclic peptides, show an excellent ability in binding many different kinds of biological targets, while mimicking the affinity and the specificity of proteins. For these characteristics and their versatility, they can be successfully employed as therapeutics and chemical probes (enzyme inhibitors, PPI inhibitors and receptor agonists and antagonists) in drug targeting and in imaging and diagnostics.[56]

Concerning cancer treatment and diagnosis, they have played a central role in recent years, while gaining an increasing interest by the scientific community, as proven by the numerous research works.[**references, such as 57-61**] As an example, specifically designed bicyclic peptides have been used to target and inhibit the epidermal growth factor receptor (HER2), which is over-expressed in 15–30% of breast cancer patients.[57] Other peptides were developed aiming at inhibiting the receptor Notch1, whose deregulation is associated to many tumor forms.[58] Another example deals with a bicyclic peptide employed as bioreceptor for an antibody, CD55, whose overexpression can lead to lung, gastric, breast, prostate, and cervical cancer.[59] Another one was developed to bind the tumor-related prostate-specific membrane antigen (PSMA), a metalloprotease.[60]

Some antibody-mimicking bicyclic peptides were also tested in binding affinity with Gastrin17, a trophic factor involved in gastrointestinal tumors, included pancreatic cancer.[61] Different synthetic bicyclic peptides, which are illustrated in **Figure 16**, were tested on growth factor receptor bound protein 7 (Grb7).[62] These are only few examples of the potential applications of these molecules in diagnosis and therapy for cancer.

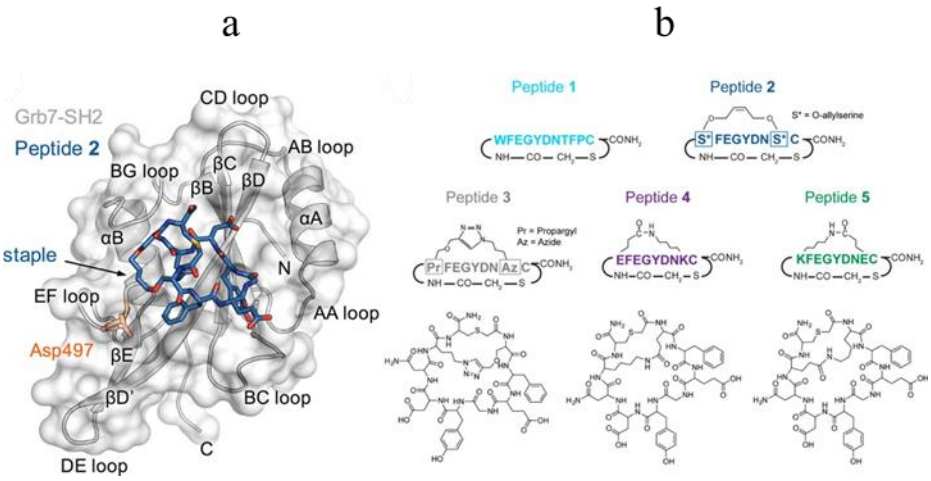


**Figure 16.** (a) X-ray structures of Grb7-SH2 domain of protein Grb7 (Growth factor receptor bound protein 7), a tumoral biomarker (grey surface), with a synthetic bicyclic peptide (blue sticks) bonded to it and (b) the aminoacidic structures of this last one and of other four different ones tested as inhibitors.[62]

## 1.5.2 Bicyclic peptides as bioreceptors in h-uPA detection

Bicyclic peptides have found promising results also in the recognition and inhibition of the urokinase plasminogen activator (h-uPA). Several peptides were synthesized and tested to compare their affinity with other two linear peptides, upain-1 and upain-2, obtaining a higher entropy loss in the interaction with uPA.[63, 64] One of the most interesting bicyclic peptides studied in recent years, called UK-18, showed high selectivity and inhibition potency ($K_i$ = 53 nM), overcoming those of tripeptide CJ-463 ($K_i$ = 20 nM)[65] and upain-1 ($K_i$ = 29.9 μM at pH = 7, T = 37 °C).[64] The main reason for its great affinity with h-uPA is due to the large interaction surface, around 701 A°, and to the numerous hydrogen bonds and complementary charge interactions.

Furthermore, the bicyclic UK-18, which structure and interaction with h-uPA are shown in **Figure 17**, resulted more potent than its monocyclic version ($K_i$ = 383 ± 37 nM) and even more than its linear one ($K_i$ = 17.5 ± 0.7 μM).[66]

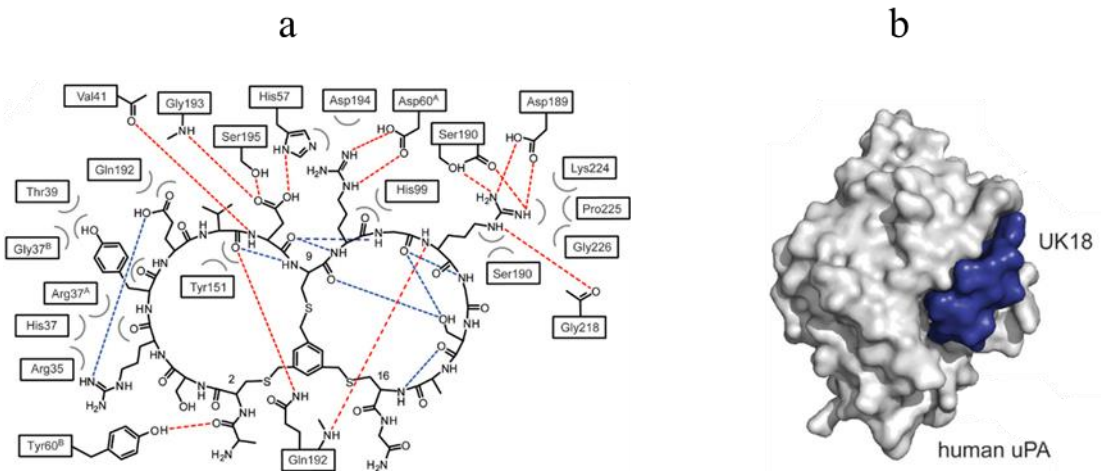


**Figure 17.** (a) Scheme of UK-18 aminoacidic structure and the molecular bonds with h-uPA (in red are shown the intermolecular ones, while in blue the intramolecular ones). (b) Crystal structure during their interaction (in grey the h-upA and in blue the peptide).[66]

The high binding capacity showed by this kind of molecules brought the attention of researchers on a possible integration as bioreceptor in cancer diagnostics. In fact, very recently two biotinylated bicyclic peptides, namely $P_1$ and $P_2$, were employed as bioreceptors for h-uPA in an electrochemical assay (see **Figure 18**). The results were very promising in terms of reproducibility, selectivity and sensitivity with LODs of 105.8 ng/mL and 32.5 ng/mL for $P_1$ and $P_2$, respectively, which are close to the nanomolar concentration range required for diagnostic purposes (see Chapter 1.2.2).[67]

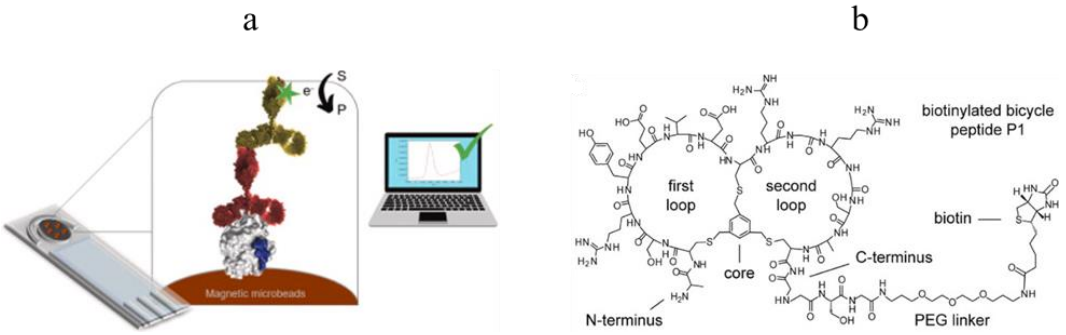


**Figure 18.** (a) Schematic representation of the DPV-based biosensing platform designed for h-uPA detection. (b) The aminoacid sequence of the bicyclic peptide $P_1$.[67]

## 1.6 Aim of the Thesis

This Thesis project aims at developing an electrochemical biosensor based on a synthetic bicyclic peptide, $P_3$, as bioreceptor for the detection and recognition of the cancer biomarker h-uPA to obtain important diagnostic information about the birth and the growth of different cancer forms, especially breast cancer. As described previously, the levels of h-uPA in serum or in tissues are linked to cancer-related biological activities and tumor evolution. Therefore, developing a novel biosensing platform and methodology could find important applications in oncological diagnostics. The platform is designed to be user-friendly and portable, thus avoiding the need for core facilities and qualified personnel to run the tests. Bicyclic peptides have recently emerged as good candidate to develop synthetic receptors in biosensing. Besides their ease in production and their stability, they have shown high binding affinity and good performances in electrochemical biosensing platforms specifically devised for h-uPA. The performances of the synthetic bicyclic peptide in exam ($P_3$) were compared to those of a previous one ($P_2$) in a labeled sandwich-like electrochemical immunoassay. The same receptor was also implemented in a novel label-free impedimetric platform design, which was characterized providing promising results in the detection of h-uPA.

# 2. Experimental section

## 2.1 Reagents and solvents

Alanine (A), cysteine (C), serine (S), arginine (R), phenylalanine (F), valine (V), aspartic acid (D), glycine (G), proline (P), Fmoc-PEG-Biotin Novatag™ (NovaBioChem™) resin, dimethylformamide (DMF), piperidine, dichloro methane (DCM), N-methyl-2-pyrrolidone (NMP), N-methylmorpholine (NMM), acetic anhydride, 2,6-Lutidine 6%, benzotriazol-1-yloxytripyrrolidinophosphonium hexa-fluorophosphate (PyBOP) activator, trifluoro acetic acid (TFA), anisol ($CH_3OC_6H_5$), 1,8-octadiol ($(CH_2)_8(OH)_2$), thioanisol, diethyl ether, acetonitrile ($CH_3CN$), ammonium carbonate ($((NH_4)_2CO_3$), acetonitrile ($CH_3CN$), 1,3,5-Tris(bromomethyl)benzene (TBMB), hydrochloridric acid (HCl), tris(hydroxymethyl)aminomethane hydrochloride (tris-HCl or Trizma-HCl), diethanolamine (DEA), non-ionic polyoxyethylenesorbitan monolaurate (Tween 20), potassium hexacyanoferrate(II) trihydrate, Anti-Rabbit IgG-Alkaline phosphatase secondary antibody (Ab2-ALP), 1-Naphtyl phosphate disodium salt (1-NPP) and biotin were purchased from Sigma-Aldrich (Merck).

Ethylendiaminotetraacetic acid (EDTA), magnesium chloride hexahydrate ($MgCl_2•6H_2O$) and monobasic potassium phosphate ($KH_2PO_4$) were purchased from AppliChem (Biochemica).

Potassium hexacyanoferrate(III) and potassium chloride (KCl) were purchased by VWR® BDH® Prolabo.

Dihydrate dibasic sodium phosphate ($Na_2HPO_4•2H_2O$) and sodium chloride (NaCl) were purchased from CARLO ERBA Reagents S.r.l. Dynabeads® MyOne™ Streptavidin C1 magnetic microbeads (MB) and the urokinase polyclonal primary antibody (Ab1)were purchased from Invitrogen™-Thermo Fischer.

The ultra-pure Milli-Q water used in all the procedures was obtained with MilliQ Gradient (Millipore).

Low molecular weight human-urokinase plasminogen activator (h-uPA) was gently provided by Prof. Laura Cendron, University of Padua.

The Binding and Washing 2X (B&W 2X) buffer at pH = 7.5 was prepared by mixing Tris-HCl solution at pH = 7.5 (10 mM), EDTA at pH = 8.0 (1 mM) and NaCl (2 M) in MilliQ water.. Phosphate Buffer Solution (PBS) (0.5 M) at pH = 7.0-7.4 was prepared with $Na_2HPO_4$ (3.97 mM), $KH_2PO_4$ (1.46 mM), NaCl (136 mM) and KCl (2.68 mM) in MilliQ water. DEA buffer solution was obtained adding diethanolamine (DEA) (0.1 M), KCl (0.1 M) and $MgCl_2•6H_2O$ (1 mM) to MilliQ water. Binding and Washing buffer 1X (B&W 1X)/Tween 20 (0.01 %), Phosphate Buffer Solution (PBS) (0.5 M)/ Tween 20 (0.01 %) and DEA/Tween 20 (0.01 %) were made adding 0.01 g/mL of Tween 20 to PBS (0.5 M), Binding and Washing buffer 2X (B&W 2X) and DEA buffer solutions, respectively. Binding and

Washing buffer 2X (B&W 2X) were previously diluted 1:1 ratio with MilliQ water to obtain Binding and Washing buffer 1X (B&W 1X).

The $[Fe(CN)6]^{3-/4-}$ solution (1 mM) , used in the impedimetric (EIS) measurements, was prepared by mixing potassium hexacyanoferrate(II) trihydrate and potassium hexacyanoferrate(III) in the PBS (0.5M) buffer, previously prepared.

## 2.2 Instrumentation and methods

*Synthesis*. To synthetize the linear peptide $P_3$, an automatized synthetizer, INTAVIS™ ResPep SLi, adopting the Solid-Phase Peptide Synthesis (SPPS).

For the peptide purification and fractioning processes, a Waters Prep LC Preparative Chromatography System was used which consists in Waters PrepLC System (preparative mode), Waters PrepLC Controller, Waters Waters UV/Visible Detector 2489, Waters Fraction Collector III and as preparative column a Luna 10 µm C18(2) 100 Å, LC Column 250 x 10 mm by Phenomenex. The operational parameters were set as follows: flow rate at 4 mL $min^{-1}$; wave length of UV/Visible detector lamp at $\lambda_1$ =220 nm and $\lambda_2$ =280 nm. The mobile phase was composed of eluent A (99.9% v/v $H_2O$ and 0.1% v/v TFA) and eluent B (99.9% v/v acetonitrile (ACN) and 0.1% v/v TFA). The raw peptide was dissolved in a solution $H_2O$/ACN (10% v/v). The injection volume of samples was 800 µL. The analyses were carried out with a linear concentration gradient of eluent B in A from 10% to 90% for 23 minutes.

For the centrifugation operation, a HeraeusTM MultifugeTM X1R centrifuge by Thermo-Fischer (4000 rpm, 10 min, 5 °C) was used.

The peptide freeze-drying processes were carried out with a freeze-dryer LIO5P from Cinquepascal S.r.l (pressure: 0.3 mbar, range temperature: -40 °C/ - 50 °C).

*Mass spectrometry*. The mass spectra analysis of the linear and the bicyclic peptide were conducted with an electrospray ionization (positive polarity) mass spectrometry (ESI–MS) performed on a single quadrupole liquid chromatograph InfinityLab LC/MSD mass spectrometer (Agilent Technologies) coupled to a reversed-phase 1260 Infinity II LC system (Agilent Technologies) with a column NUCLEOSIL 100-5 C18 (5 µm, 125 mm × 4 mm; Macherey-Nagel). The runs were carried out at a flow rate of 1.00 mL $min^{-1}$ with a linear gradient of mobile phase of eluent D (99.9% ACN and 0.1% v/v HCOOH) into eluent C (99.9% v/v $H_2O$ and 0.1% v/v HCOOH) from 10% to 100% in 20 minutes. For the mass analysis of the peptide samples were made solutions of $H_2O$/ACN (10 % v/v). The obtained data were acquired with Agilent OpenLAB CDS (Agilent Technologies), then processed and analyzed with MestReNova (Mestrelab Research).

*Electrochemistry*. The electrodes used for the in the experiments were the Screen-Printed Carbon Electrodes (SPCE; Ref. 110) and the Streptavidin modified Screen-Printed Carbon Electrodes (Strep-SPCE; Ref. 110STR), both from Metrohm DropSens.

The voltametric measurements were performed with a portable potentiostat EmStat Blue by PalmSens, employing an electrode connector from Metrohm DropSens and PSTrace as data analysis program. The optimized DPV parameters were set as follows: initial potential = -1 V, end potential = +0.65 V, step potential = 0.002 V, modulation amplitude = 0.002 V, scan rate = 0.05 V/s and equilibration time = 10 s.

The the impedimetric measurements were carried out with a SP-300 dual channel potentiostat by BioLogic featuring the EIS module and ECLab program to collect the experimental data. The PEIS (Potentio Electrochemical Impedance Spectroscopy) measurements were performed by setting the instrument parameters as reported in a previous similar case study:[68] frequency range = 0.1 MHz – 0.1 Hz and sinus amplitude = 10 mV.

The solutions were mixedby means of a ZX3 Advanced Vortex Mixer from Velp Scientifica® and a HulaMixer® Sample Mixer from Life Technologies™ (Thermo-Fischer).

*Other software employed*. The graphs presented herein were plotted using OriginLab® program. The aminoacidic structures of peptide $P_3$ (**Figure 19** and **Figure 20**) were designed with ChemDraw Professionals 15.0 program.

## 2.3 Synthesis and characterization of the peptide $P_3$

The peptide $P_3$[69] was prepared using an SPPS (Solid-Phase Peptide Synthesis*)* synthesizer, INTAVIS™ ResPep SLi. This technique uses a solid support where the amino acids, which are added in excess, can undergo a condensation reaction leading to the desired the peptide. This technology can provide high yields, short times of execution and lower production costs. The chosen solid support was the Fmoc-PEG-Biotin Novatag™ by Merck KGaA-Sigma–Aldrich, that includes polyethylene glycol (PEG) and biotin that will be part of the peptide structure. The F-moc group (9-fluorenyl-methyloxy-carbonyl) was removed during the process. The substitution rate of the resin is 0.35 mmol of peptide/grams of resin. The right amount of resin to weight was calculated as it follows, by taking into account that 6 cartridges can produce 10 µmol of peptide each:

$$\text{g of resin} = \frac{\text{mmol of peptide for each cartridge}}{\text{substitution rate of the resin}} = \frac{0{,}01\ \text{mmol}}{0{,}35\ \text{mmol/g}} = 0{,}029\ \text{g} = 29\ \text{mg}$$

The software directly calculated the amounts in grams for every amino acid of the chosen sequence and the right volumes of solvent, DMF, for each one of them, as it is reported in **Table 1**.

| Amino acid | Calculated weight (mg) | Real weight (mg) | DMF solvent volume (mL) |
|---|---|---|---|
| Alanine (A) | 390 | 394.6 | 2.27 |
| Arginine (R) | 1720 | 1725.8 | 4.27 |
| Glycine (G) | 996 | 1002.6 | 6.10 |
| Aspartic acid (D) | 515 | 517.2 | 2.19 |
| Cysteine (C) | 1553 | 1554.5 | 4.37 |
| Phenylalanine (F) | 485 | 490 | 2.21 |
| Proline (P) | 422 | 430 | 2.25 |
| Serine (S) | 480 | 489 | 2.21 |
| Valine (V) | 662 | 663.3 | 2.50 |

**Table 1.** Software calculated weights, real weights and DMF volumes for the amino acids that assemble the peptide P3.

The aminoacidic sequence of the peptide $P_3$ is the following:

A C S R F V V D C R G R G G P C G

The procedure consists in cycles, one for each addition of amminoacid, made by three steps:

1) *Deprotection*: the protecting group F-moc is removed in alkaline condition using the piperidine solution (20% v/v in DMF) for 30 minutes.
2) *Coupling*: the first aminoacid of the sequence links to the deprotected resin and the next aminoacid links to the previous one, both via the formation of peptide (amidic) bond using the activator PyBOP (9.6 g, 0.5 M in 37 mL in DMF), NMM (4M) and NMP (5 mL).
3) *Capping*: to deactivate the remaining active sites after the coupling, acetic anhydride solution (5% v/v in DMF, 0.53 M) is added.

These three steps are repeated for each aminoacid added and upon each cycle there is a final washing step. At the end of the synthesis, a cleavage step to separate the biotinylated linear peptide from the resin was performed for 3 hours using TFA (trifluoro acetic acid 95% v/v) solution, which also contains water (2.5 % v/v), anisol (2.5% v/v), 1,8-octadiol (2.5 % v/v) and thioanisol (2.5 % v/v). For the cleavage step, 3 different syringes (1 for 2 cartridges employed) were used and kept in continuous agitation. Then the peptide was washed for 3 times with 50 mL of cold diethylether (-25 °C), dissolved in a solution of ACN/$H_2O$ 1:1 and lyophilized.

The linear peptide structure is illustrated in **Figure 19**:

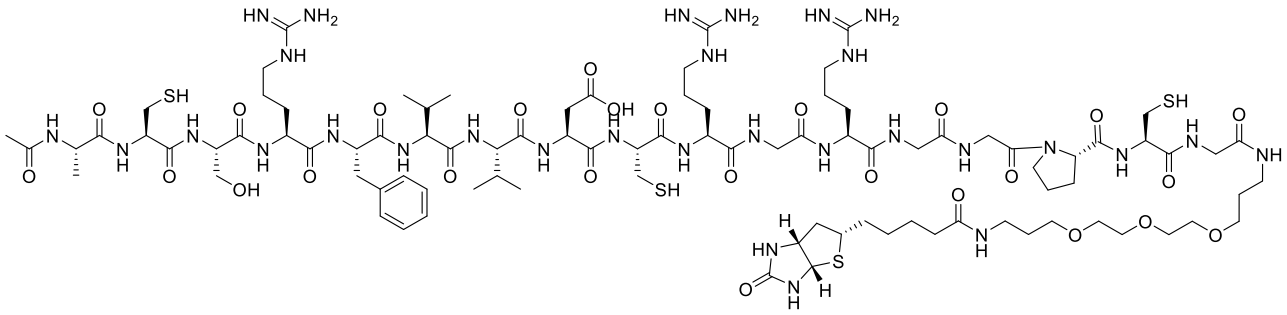

**Figure 19.** Linear biotinylated peptide $P_3$ structure.

From the structure, illustrated in **Figure 19**, at the right extremity the biotin and the PEG linker, both deriving from the Fmoc-PEG-Biotin resin used in the SPPS synthesis. The biotin plays a fundamental role in the assembly of the biosensing platforms described in this Thesis work as it allows the peptide to bind to the Streptavidin-modified surfaces. Once the linear peptide is ready, it has to undergo bicyclization. First the lyophilized peptide is dissolved in a 1 mM solution of $NH_4HCO_3$ (70% v/v) and ACN (30 % v/v) at pH = 8. Then 1.5 mM of the cyclizing alkylant agent, TBMB(previously dissolved in a little volume of acetonitrile) is added and left to react 1 hour. The addition of 5 µL of HCl (3M) halted the reaction. The last step was the purification of the biotinylated bicyclic peptide via reverse phase HPLC (Semi-prep LC). All the fractions associated to a specific signal in the chromatographs were collected and analyzed via HPLC/MS mass spectroscopy. The bicyclic biotinylated peptide samples (MW= 2323.09 g/mol) were then lyophilized, weighted and stored at -20 °C. A final mass of 4.4 mg of P3 were obtained.The bicyclic structure of $P_3$ is depicted in **Figure 20**.

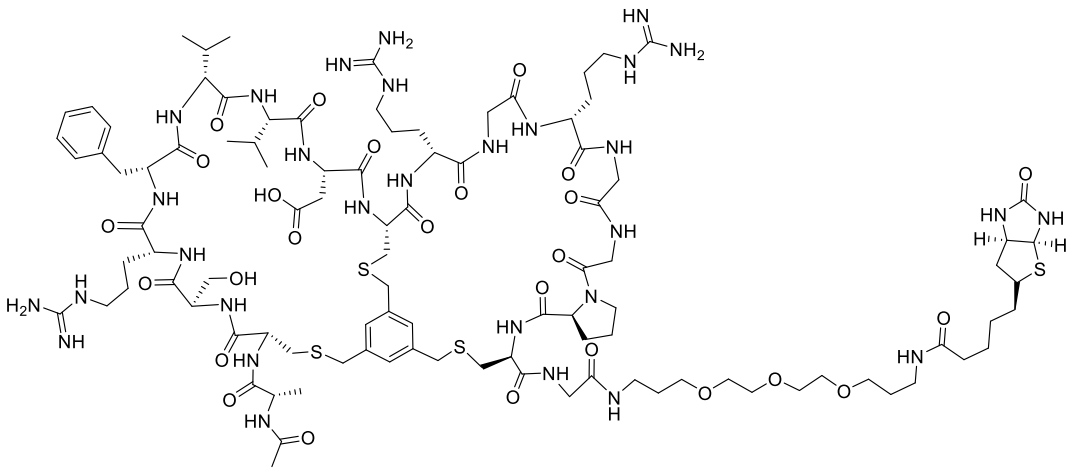

**Figure 20.** Biotinylated bicyclic peptide $P_3$ structure. The TBMB residue can be observed in the center of the structure, where its original bromide groups are substituted with the sulfide ones deriving from the cysteines present in the peptide structure. This allows to obtain two cycles and then the wanted bicyclic form.

## 2.4 Magnetic microbeads functionalization with peptide $P_3$

From the stock solution 25 μL of the Dynabeads® MyOne™ Streptavidin C1 MB were taken (10 mg $mL^{-1}$) and put in a 1.5 mL Eppendorf tube. The binding capacity to the beads for biotinylated peptides is expected to be 400 pmoles/mg, according to the manufacturer. Therefore, 25 μL can potentially bind 100 pmoles of peptide $P_3$. The PBS solution, where the MB were suspended, was removed, and the latter ones were washed first with 200 μL of B&W 2X, B&W 1X/Tween 20 (0.01 %) and then with 200 μL of PBS (0.5 M)/Tween 20 (0.01 %) in this order. Each washing step consist in adding the buffer, vortex for few seconds to resuspend the MB and then leave the Eppendorf tube in the magnetic rack for 2 minutes, before removing the first buffer and adding the second. 0.5 mg of the bicyclic biotinylated peptide $P_3$ were dissolved in 1 mL of MilliQ water to provide a 0.5 μg $mL^{-1}$ solution. 3 μL of the latter peptide stock solution (0.5 μg $mL^{-1}$) and 197 μL of PBS (0.5 M) buffer solution were added in the Eppendorf tube containing the MB, and left incubating in a rotary shaker for 30 minutes. Afterward, the unreacted peptide solution was removed by magnetic separation and stored at -20 °C. Whereas the MB functionalized with $P_3$ underwent two washing steps, both with PBS(0.5M)/ Tween 20(0.01 %). Then 200 μL of a freshly prepared 1 mM biotin solution in PBS (0.5 M) were added to the beads in excess to saturate the possible remaining Streptavidin active sites and left in incubation in a rotary shaker for other 30 minutes. Then the unreacted biotin solution was removed, put in another vial and stored in the fridge at +5 °C. Eventually other two washing steps were performed, both with PBS(0.5 M)/Tween 20(0.01 %). Finally 200 μL of PBS(0.5 M)/Tween 20(0.01 %) were added to resuspend the MB, which were stored in the fridge at +5 °C prior to use.

## 2.5 Assembling procedure of the voltametric MB-based biosensing platform

First, the spiked human-urokinase plasminogen activator (h-uPA) solutions in PBS (0.5 M) buffer were prepared by diluting the stock solution. The concentration range was from 0.1 μg $mL^{-1}$ to 1 μg $mL^{-1}$. For each spiked sample solution an equal number of Eppendorf tubes containing 15 μL of the functionalized MB/$P_3$ were prepared Once a washing step with 200 μL of PBS (0.5 M) buffer was performed, 200 μL of h-uPA spiked sample solution was added to each of them and left incubating in the rotary shaker for 20 minutes. Afterwards, the adduct MB/$P_3$/h-uPA were separated on a magnetic rack for 2 minutes. The unreacted h-uPA solutions were removed and 3 washing steps were performed, 2 with PBS(0.5 M)/Tween 20 (0.01 %) and 1 with PBS (0.5 M). Then 100 μL of the $Ab_1$ solution (2 μg $mL^{-1}$), freshly prepared from the stock one, were added to each vial containing the MB/$P_3$/h-uPA and left incubating in the rotary shaker for 15 minutes. The unreacted Ab1 solutions were magnetically separated for 2 min, collected in a vial and stored in the fridge at +5 °C.

After 3 washing steps, 2 with DEA/Tween 20 (0.01 %) buffer and 1 with DEA buffer, 200 µL of the $Ab_2$-ALP solution, freshly prepared from the stock one, were added. The samples were left incubating in the rotary shaker for 15 minutes and then magnetically separated for 2 minutes to remove the unreacted antibody solution, which was collected and stored in the fridge at +5 °C. To conclude, 50 µL of DEA buffer were added to the MB/$P_3$/h-uPA/$Ab_1$/$Ab_2$-ALP solution and used to carry out the electrochemical measurement. Prior to the DPV analysis, the active substrate 1-NPP solution (0.5 $\mu gmL^{-1}$) was prepared and put for 5 minutes in the rotary shaker. This solution must be made not more than 30 minutes before the measurements and stored in a cold and dark place, because the substrate is sensitive to hydrolysis by light. The SPCE electrode was rinsed thoroughly with MilliQ water and connected to the potentiostat. A magnet was posed under the SPCE in contact with the bottom face. This was necessary to make sure that the magnetic beads undergo magnetic deposition only on the working electrodes. 60 µL of the substrate solution and 10 µL of the MB/$P_3$/h-uPA/$Ab_1$/$Ab_2$-ALP solution were gently deposited on the working electrode surface. After 5 minutes of incubation, where the 1-NPP become 1-Naphtol (1-NP) for the dephosphorylation by the alkaline phosphatase in $Ab_2$-ALP, the DPV measurement was carried out. In **Figure 21** the main steps of this assembling procedure, as previously described,[67] are illustrated.

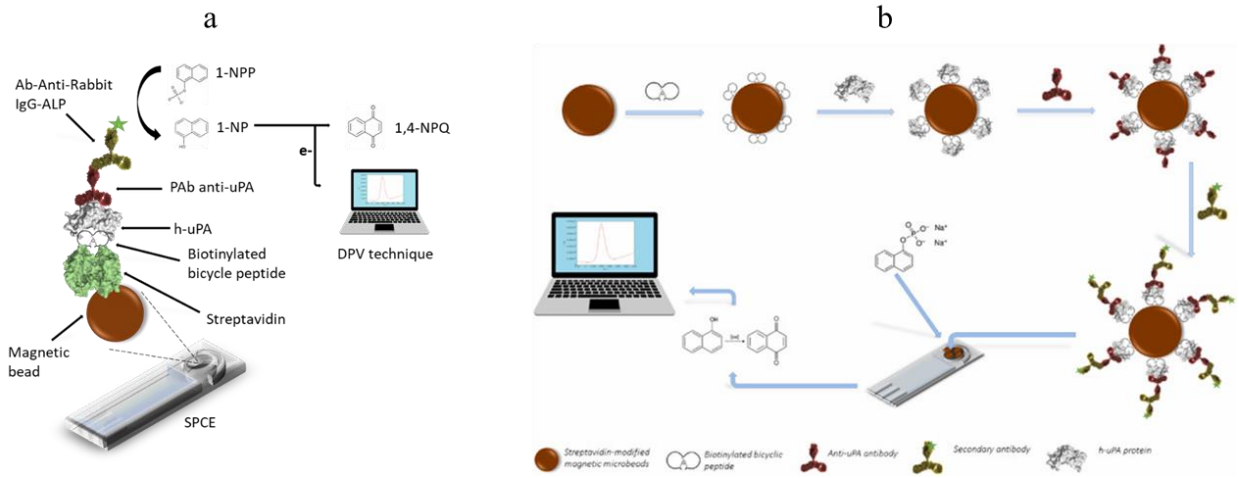


**Figure 21**. (a) Scheme of the bicyclic peptide-based biosensing platform architecture for voltammetric analysis and (b) its assembling procedure.[67] After MB are functionalized with $P_3$, s, h-uPA is captured by the peptide. Successively $Ab_1$ and $Ab_2$-ALP are added. Then alkaline phosphatase (ALP) dephosphorylates the substrate 1-NPP in 1-NP, which is electrochemically active and undergoes oxidation to 1-NPQ, thus generating the current that allows detecting the concentration of h-uPA via DPV analysis.

## 2.6 Assembling procedure of the impedimetric Streptavidin-SPCE based biosensing platform

An equal number of Strep-SPCEs as the spiked h-uPA samples were put on a Petri's plate on ice and rinsed with 100 µL of MilliQ water and gently dried with Argon (Ar) flux. Two washing steps were made, in the same way as described in the **Section 2.4**, with PBS (0.5 M)/Tween 20 (0.01 %) and PBS(0.5 M). For each Strep-SPCE an EIS measurement was performed. The analysis procedure consists of connecting the Strep-SPCEs to the potentiostat, adding 80 µL of the probe solution, $[Fe(CN)6]^{3-/4-}$ (1 mM) in PBS(0.5 M), on the working electrode and start the EIS measurement. Successively the probe solution was removed from the electrodes and other two washing steps with PBS (0.5 M)/Tween 20 (0.01 %) and PBS (0.5 M) buffers were carried out in this order. On each working electrode only 20 µL of the peptide $P_3$ solution (5 µg $mL^{-1}$) in PBS (0.5 M), previously prepared from the stock one, were added and incubated for 30 minutes. Afterwards, the $P_3$ solution droplets were removed and the SPCEs were washed two times with PBS (0.5 M)/ Tween 20 (0.01 %) and PBS (0.5 M) buffers. Then a second EIS analysis with the probe solution was performed. Upon removal of the probe solution droplet, the electrodes underwent two washing steps with PBS (0.5 M)/Tween 20 (0.01 %) and PBS (0.5 M) buffer. Then 20 µL of the spiked h-uPA solutions in PBS (0.5 M) were added and incubated for 30 minutes followed by two washing steps as previously described, prior to carrying out the final EIS measurements with the probe solution. In **Figure 22** the main steps of this assembling procedure of the impedimetric biosensing platform are illustrated.

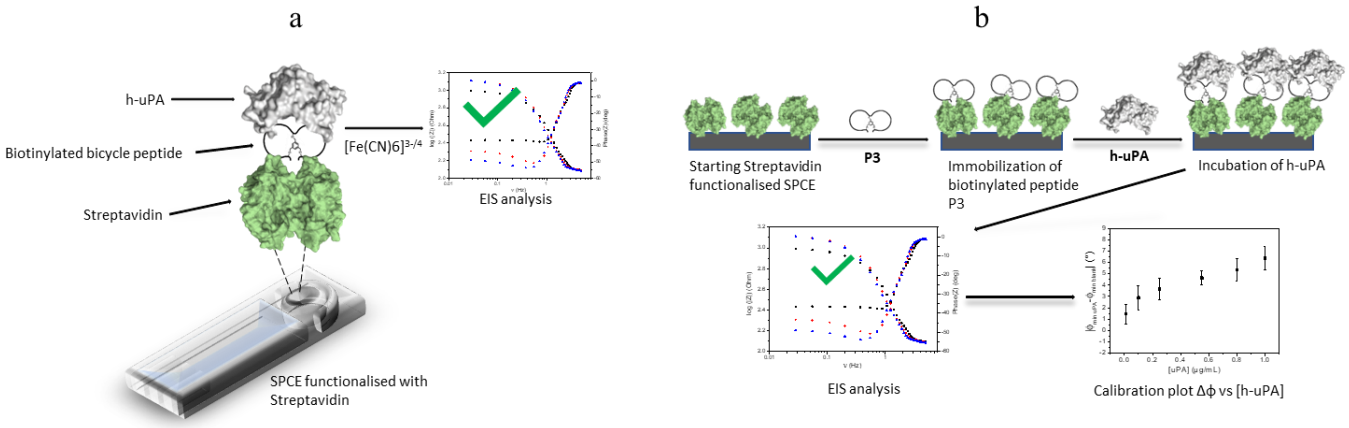


**Figure 22**. (a) Scheme of the impedimetric Streptavidin SPCE-based biosensor for h-uPA and (b) its assembling scheme.

# 3. Results and discussions

## 3.1 Characterization of biotinylated bicyclic peptide $P_3$

As describe in the experimental section, $P_3$ was purified and characterized by HPLC/MS and the chromatogram is shown in **Figure 23**.

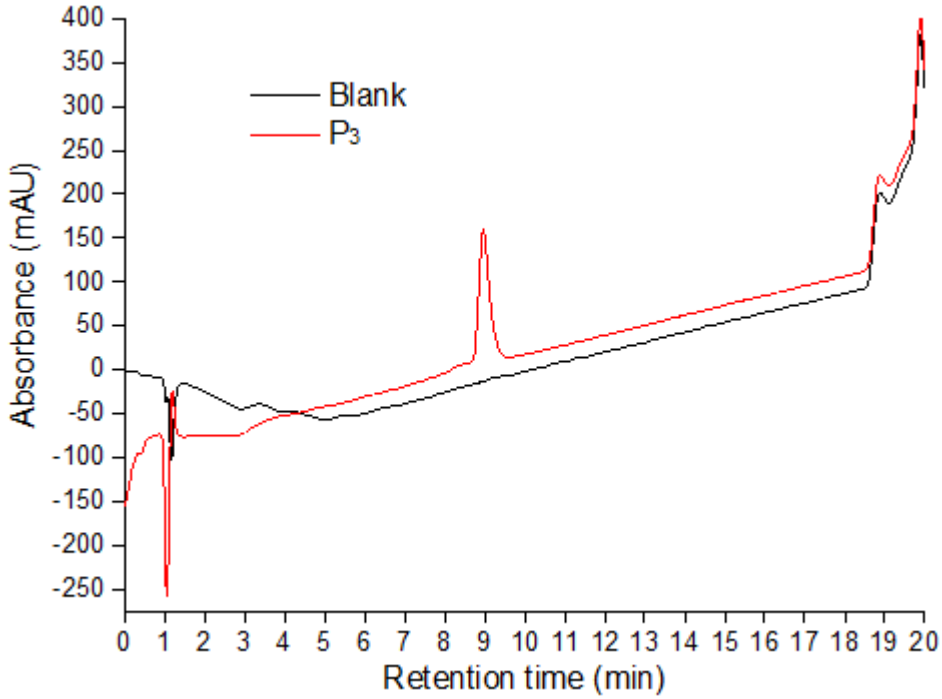


**Figure 23.** Chromatogram of the peptide $P_3$ sample (red line) and the one containing only the eluent (black line).

The sharp peak with a retention time of about 9 minutes is absent in the analysis of the solvent alone, witnessing that the only detected species is our sample. The purity was calculated and resulted > 95%.

Mass spectrometry analysis, shown in **Figure 24,** confirmed that the eluted compound was indeed the biotinylated bicyclic peptide $P_3$, whose molecular weight has a theorical value of 2323.09 g/mol.

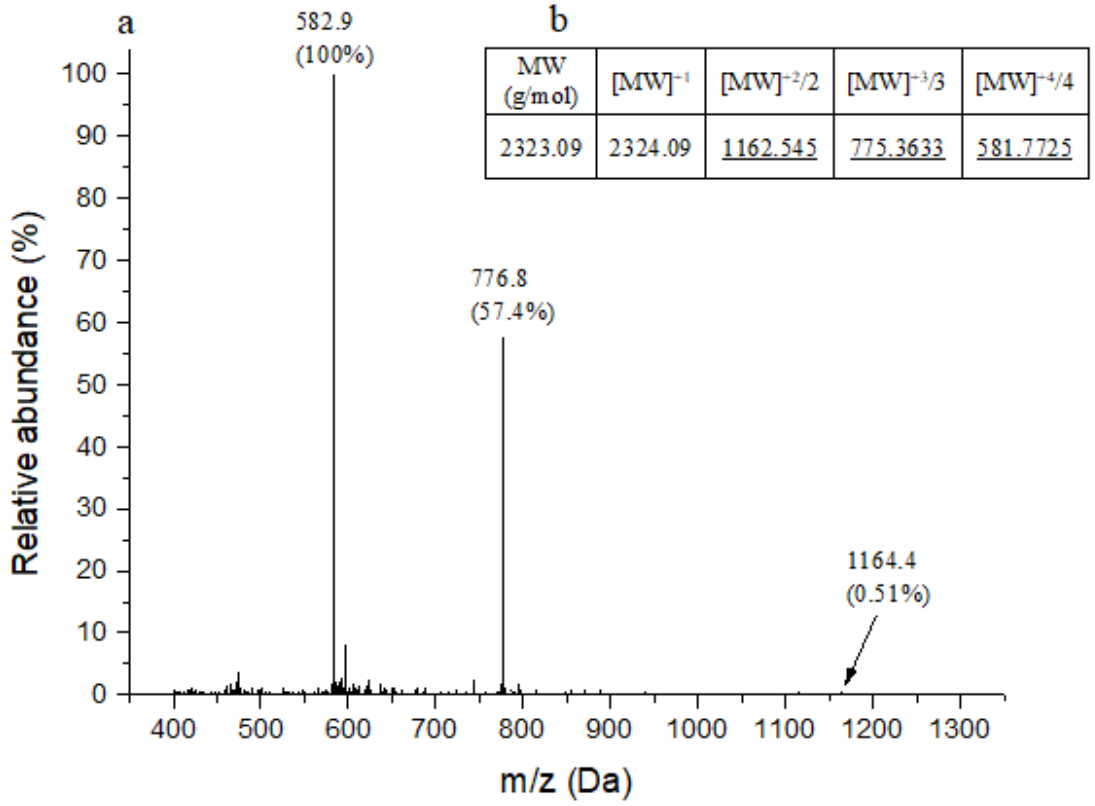


**Figure 24.** (a) MS spectrum of the chromatographic peak (8.55-9.57 min) of $P_3$ and (b) theorical fragment ions (m/z ratio) calculated from the molecular weight of peptide $P_3$.

In **Figure 24a** the two most intense signals (582.9 m/z and 776.8 m/z) and the one at 1164.4 m/z in the MS, highlighted with their m/z ratio values are coherent to the theorical ones shown in **Figure 24b.**

## 3.2 Comparing $P_3$ and $P_2$ performance in voltammetric assay

The whole assembling procedure of the bicyclic peptide-based voltametric biosensor was already described in a previous article.[67] The inhibitory activity toward h-uPA of the *ad hoc* synthetized bicyclic peptides $P_3$ and $P_2$ was previously characterized in solution with a fluorescence-based assay and $P_3$ activity was found to be double than that of $P_2$.[67, 69] Despite the minimal variation in the amino-acid sequences (3 amino acids) between $P_2$ and $P_3$, the increased inhibitory activity of $P_3$ might result in higher sensitivity in the electrochemical assay.[67] However, the performances of a bioreceptor in solution or in a confined surface might dramatically change as already described for other biomolecules.[70] To verify $P_3$ binding affinity toward h-uPA in a confined surface, this biotinylated peptide was first immobilized on the surface of streptavidin-functionalized magnetic microbeads (Strep-MB) and employed in a sandwich-type affinity electrochemical assay following the protocol previously optimized for $P_2$.[67] $P_3$ is bound to the magnetic microbeads thanks to the high affinity between biotin and Streptavidin, which the surface of the magnetic microbeads is completely functionalized of. In this preliminary part of the study, $P_2$ was tested aiming at comparing the performance of the peptide-based assays in the same working conditions. For all h-uPA concentration tested, the assay with $P_3$ showed a reliable response, thus confirming the applicability of $P_3$ as synthetic bioreceptor in electrochemical sensing platform. From the results summarized in **Figure 25** and **Figure 26**, it is possible to observe that, upon incubation of $P_3$-modified Strep-MBs with increasing concentrations of h-uPA (ranging from 0.1 to 0.5 $\mu gmL^{-1}$), higher current intensities were recorded.

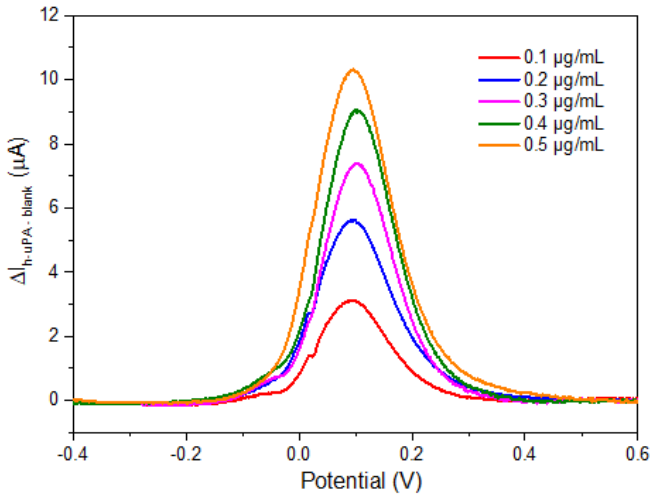


**Figure 25**. DPV peaks, subtracted to the blank, of the h-uPA concentrations tested in the linear region in the voltametric $P_3$-based platform. The potential related to each signal (≈ +0.1 V) corresponds to the oxidation of dephosphorylated substrate, 1-naphtol, into 1- naphthoquinone, that produce the currents detected successively with DPV. An increase of the signal intensity indicates a growing number of Ab2-ALP-Ab1-h-uPA-$P_3$-Strep-MB complexes, that is related to an increasing value of analyte concentration.

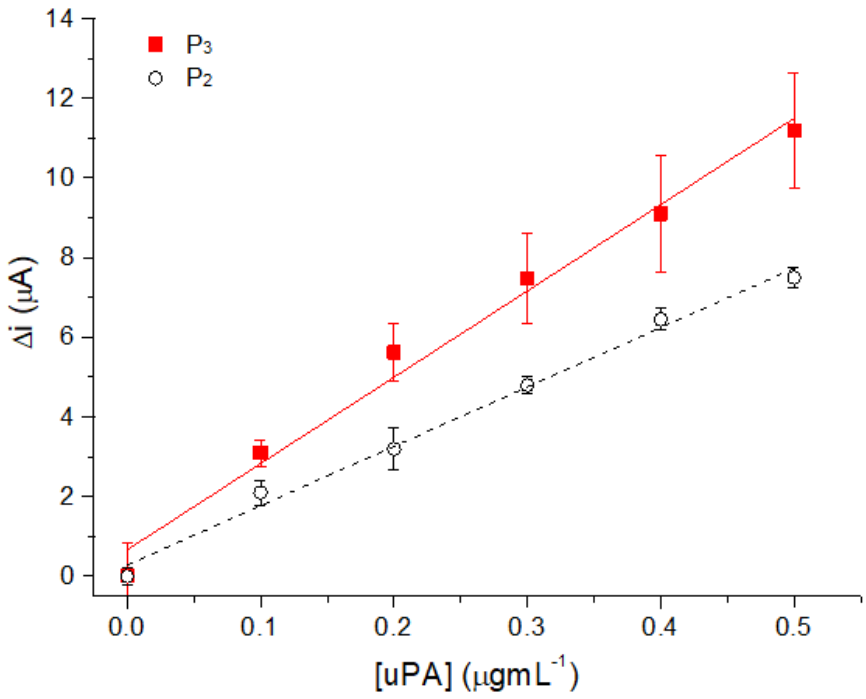


**Figure 26**. Comparison of the calibration plots of h-uPA obtained via sandwich-type affinity assay using $P_2$ (black empty circles) or $P_3$ (black full squares) modified-MB. The values presented are the average of triplicate measurements with the associate error calculated as standard deviation. The linear fitting equations for $P_2$ (dashed black line): y= 16.0±0.9x + 0.28±0.07 and P3 (black full line): 21.7±1.3x + 0.67±0.39.

With reference to **Figure 26**, $P_3$-based assay shows a higher value of the slope obtained from the linear regression of the calibration plots, when compared to $P_2$. In fact, for $P_2$ the slope value is 16.0±0.9, while for $P_3$ is 21.7±1.3. This means that for a certain concentration of h-uPA, in the $P_3$-based platform the signal is higher than for the $P_2$-based one in the same experimental conditions. Therefore, $P_3$-based assay shows a higher sensitivity compared to $P_2$. The $P_3$ trend also show the same linear range of $P_2$, which is reported in literature for the same DPV platform.[67] The dynamic range of $P_3$-based assay was further tested with h-uPA concentrations in the spiked samples ranging from 0.1 to 1 μg $mL^{-1}$. The results at concentrations of spiked h-uPA as high as 1 μg $mL^{-1}$, depicted in **Figure 27,** showed that the linear portion of the dynamic range of the platform is between 0 μg $mL^{-1}$ and 0.5 μg $mL^{-1}$, which is coherent with the one verified in the previous case study.[67] However, the trend from 0.5 μg $mL^{-1}$ and 1 μg $mL^{-1}$ is decreasing and shows a plateau which can be attributed to the Hook effect, which occurs when there is an overabundance of analyte that saturates the system.

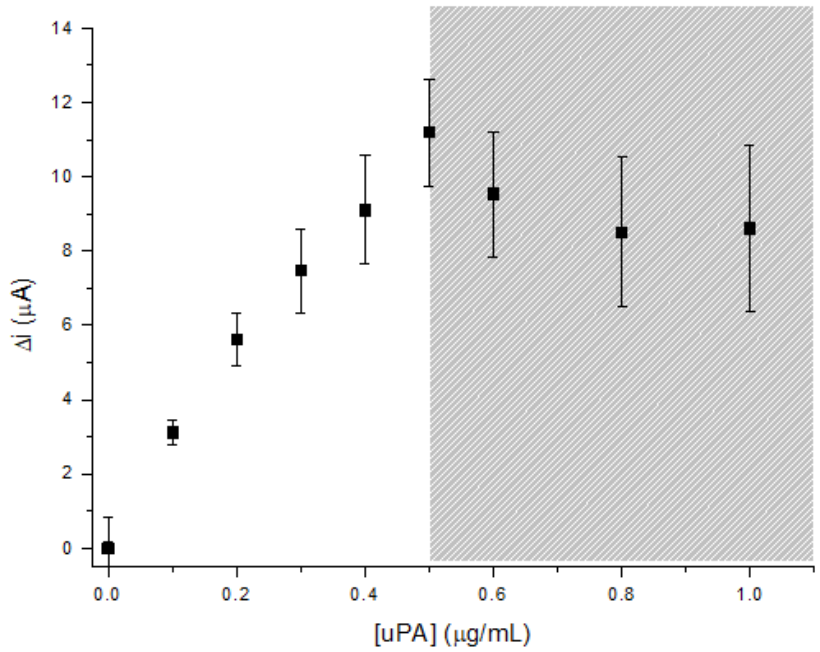


**Figure 27**. $P_3$ behavior in a wider concentration range (0.0 – 1 μg $mL^{-1}$) as bioreceptor in the DPV sandwich-like immunoassay.

The results summarized in **Figure 27** show that for h-uPA concentrations higher than 0.5 μg $mL^{-1}$ no meaningful changes in the analytical signal were recorded. This value corresponds to the experimental limit of linearity (LOL) of the calibration plot. From this data we can deduce that $P_3$-based assay allows accurately determining h-uPA concentrations lower than 0.5 μg $mL^{-1}$, while for higher h-uPA concentrations the electrochemical signal is saturated (grey region in **Figure 27**). The better binding affinity of $P_3$ to h-uPA than $P_2$, already observed by the characterization in solution with the fluorescence-based assay,[69] was confirmed by the better performance obtained also in a confined surface in the sandwich-like voltametric immunosensor.

## 3.3 EIS-based sensor design and characterization

In label-free impedance-based biosensors, electrochemical impedance spectroscopy (EIS) allows monitoring the changes in the electrical properties of the electrode-electrolyte interface when a small-amplitude sinusoidal potential wave is applied on a DC potential based electrode. Depending on the architecture of the EIS-based biosensors, it is possible to distinguish between non faradic capacitive assays, where the changes in the capacitance are followed, and faradic assays requiring the addition of a redox probe in solution or confined at the electrode surface. In most faradic assay, EIS data, especially when considering the Nyquist plot, are modelled using the electrical equivalent circuits (EECs) and correlate the target concentration with the value of the double-layer capacitance ($C_{dl}$) or the charge transfer resistance ($R_{ct}$).[71] Also, the changes in the Bode plots can be considered in the design of an EIS-based analytical strategies to simplify the data elaboration process avoiding time-consuming steps (i.e., Nyquist fitting with EEC).[68]

The possibility to determine h-uPA within a faradic impedimetric sensing approach at the surface of the modified Strep-SPCE using $P_3$ as biorecognition element was verified. The biotinylated peptide, $P_3$, was immobilized on the surface of a commercial streptavidin-functionalized screen-printed carbon electrode (Strep-SPCE) following the procedure described in **Section 2.6** and exposed to spiked h-uPA samples. The changes at Strep-SPCE/solution interface were characterized via EIS in presence of 1 mM $[Fe(CN_6)]^{3-/4-}$ in PBS. The Nyquist plots obtained at the bare Strep-SPCE and after $P_3$ immobilization and h-uPA incubation (h-uPA 0.1 μg $mL^{-1}$) are compared in **Figure 28a**, while the corresponding Bode plots are presented in **Figure 28b**.

The Nyquist plots related to the Strep-SPCE (black squares), $P_3$-Strep-SPCE (red circles) and h-uPA incubated $P_3$-Strep-SPCE (blue triangles) show an increase of the signal indicating the presence of new isolating layers at the solution-electrode interface. In the Strep-SPCE, the only contribute to impedance are the Streptavidins bonded on the surface. Whereas in the $P_3$-Strep-SPCE the peptide layer is added first and then the target protein h-uPA, which is expected to form a complex with the peptide anchored at the surface. The Nyquist plot describing the SPCE-Strep solution interface can be fitted with a standard Randles circuit including the following components: solution resistance ($R_s$), constant phase element (CPE), the resistance to charge transfer ($R_{ct}$) and the Warburg element (W). Once $P_3$ is added to the platform a second couple of CPE and $R_{ct}$ elements are added in series to the EEC circuit before the W element. These components attest for the biorecognition layer obtained immobilizing $P_3$ at the SPCE-Strep surface. The addition of the bioreceptor varies the electrode/solution interface properties.

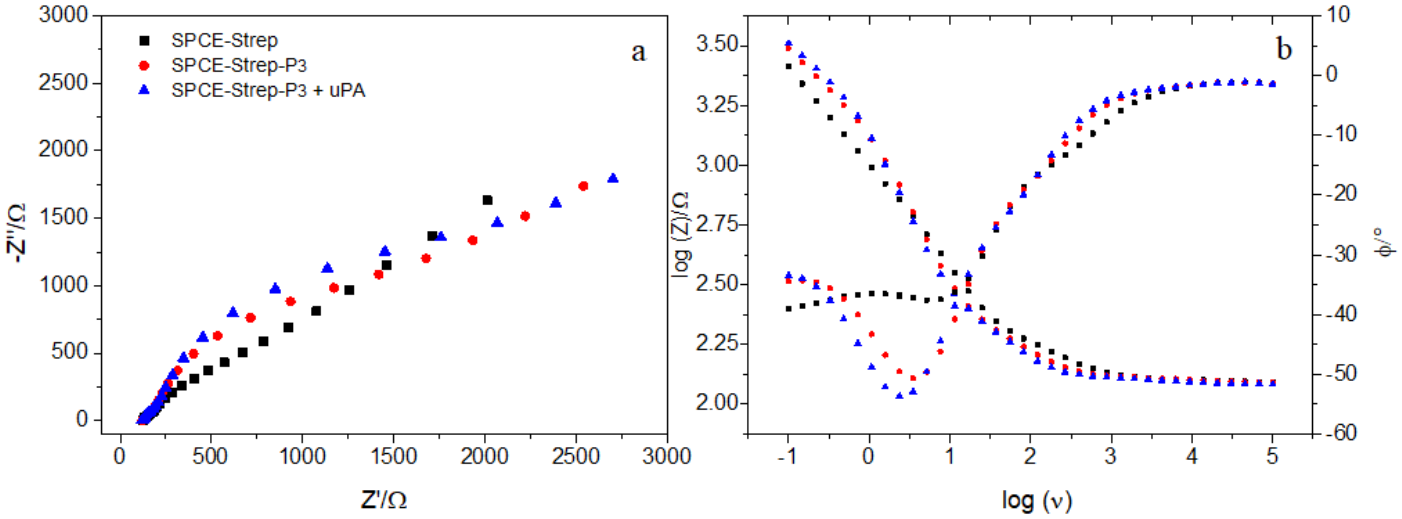


**Figure 28.** (a) Nyquist and (b) Bode plots for bare Strep-SPCE (black squares), $P_3$ modified Strep-SPCE (red circles) and $P_3$-Strep-SPCE after incubation of 0.1 μg $mL^{-1}$ of h-uPA (blue triangles). All the measurement were performed in 1 mM solution of $[Fe(CN)_6]^{3-/4-}$.

These changes can be observed even from the Bode plots, where the peaks increase progressively in phase (φ) when $P_3$ is immobilized on the electrode surface and after protein h-uPA is incubated, as shown in **Figure 28b**. Finally, the incubation of 0.1 μg $mL^{-1}$ of target protein leads to an additional interfacial layer at the SPCEs resulting in a more complex EEC circuit with supplementary CPE/$R_{ct}$ in series and an increased intensity in the process occurring at about log (ν) = 0.37 in the Bode Phase plot. The EIS characterization confirmed the successful immobilization of the bioreceptor, the formation of a stable biorecognition layer and, indirectly, its capability to recognize the target protein. Therefore, $P_3$ can be further applied in EIS-based affinity assay for the detection of h-UPA.

Prior to proceed with the preliminary tests addressing the performance of this sensing strategies, the loading of the bioreceptor was optimized. Impedimetric biosensors generally requires a high concentration of small bioreceptors like peptides.[71] In our study, different loadings of $P_3$ at Strep-SPCE were tested (0.1, 1, 5, 10, 25 and 50 μg $mL^{-1}$). To verify which one provides the highest analytical signal after the interaction with the target protein, for each of them a spiked h-uPA sample (0.1 μg$mL^{-1}$) was incubated, which is within the linear concentration range of the voltametric platform described in **Section 3.2** and in the previous article,[67]. In **Figure 29** are shown the values obtained from the normalized phase (φ) signals, deriving from Bode plots peaks, and the blank one related to each amount of $P_3$ loaded. The minimum values of the process at log (ν) = 0.37 (as showed in **Figure 28b**) in presence/absence of h-uPA were extrapolated and normalized by subtracting and then dividing the ones in presence of the target protein with the those in absence of it (blanks). We observed that the mid concentration, 5.0 μg $mL^{-1}$, was the best performing in terms of platform sensibility and peptide economy.

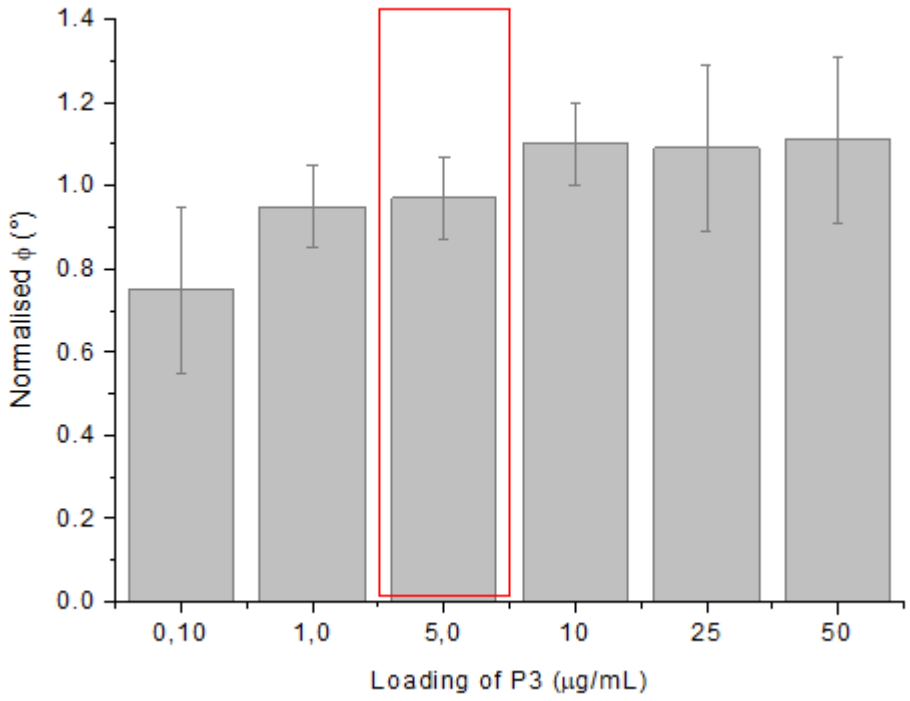


**Figure 29**. Optimization of $P_3$ loading in the impedimetric assay. Comparison of the response of the SPCE platform loaded with different concentrations of $P_3$ ranging from 0.10 to 50 μg $mL^{-1}$ in the screening of a buffer solution spiked with 0.1 μg $mL^{-1}$ h-uPA solution. The normalized phase value presented was calculated from the Bode plots. The error bars were obtained on the triplicates.

## 3.4 Impedimetric detection strategy: preliminary data

The findings of the EIS characterization study suggested the possibility of correlating the presence of h-uPA and its concentrations directly from the impedance signal, while considering the changes in the Bode phase plot peaks instead of analyzing the fitted parameters obtained from the EEC (**Figure 28b**). Subtracting the blank values, upon $P_3$ immobilization on Strep-SPCE, to the ones after h-uPA incubation (see **Figure 30**), a calibration curve could be obtained as shown **Figure 31**.

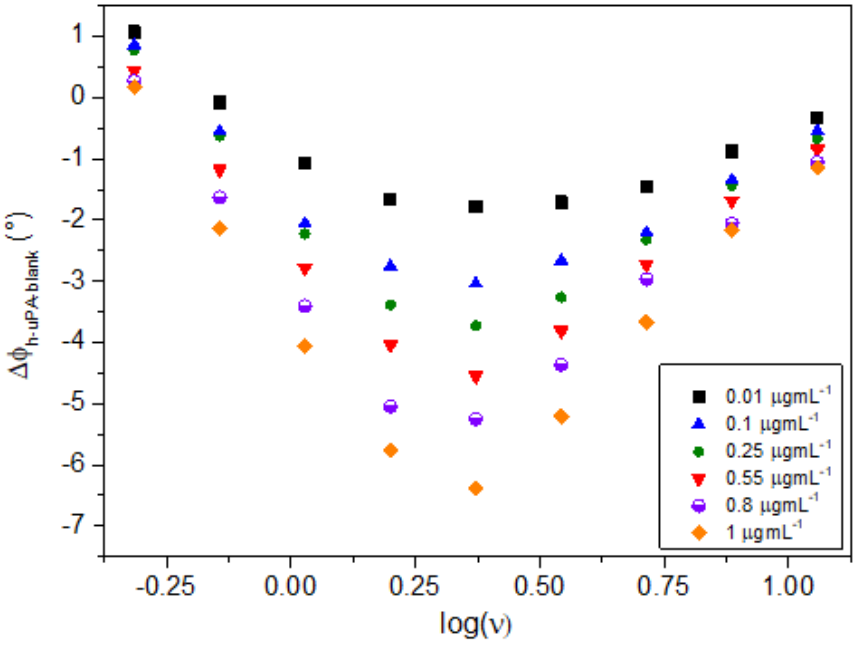


**Figure 30.** Bode plot peaks, subtracted to the blank, of the 6 tested h-uPA concentrations in the $P_3$-based impedimetric platform.

In this case a higher dynamic range (0.01-1 µg $mL^{-1}$) was explored, which showed linearity in the region 0.1-1 µg $mL^{-1}$, as depicted in **Figure 31a**. To test the platform sensibility and its possible applicability on real samples, the lower concentration range (0.01-0.1 µg $mL^{-1}$) was investigated and the results are reported in **Figure 31b**. In fact, the concentration ranges of h-uPA in human serum, which are diagnostically relevant for breast cancer, fall within this range.[17]

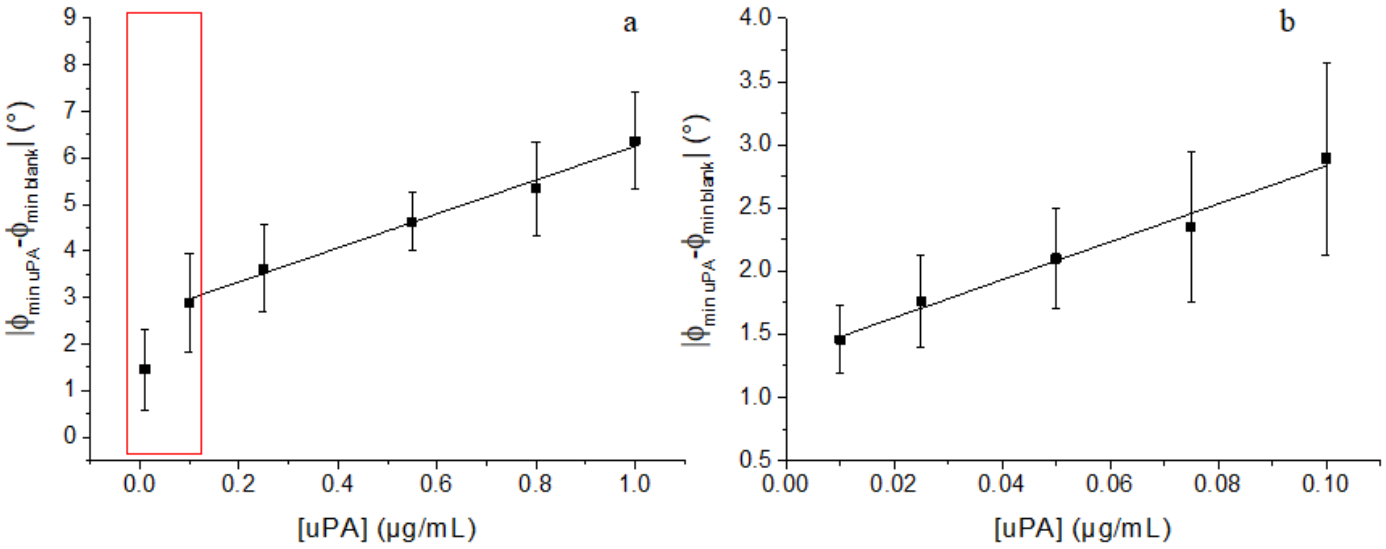


**Figure 31**. (a) Calibration plots in the h-uPA concentration range 0.01-1 µg $mL^{-1}$ of with the related Bode plots peaks with linear fitting equation (black full line): y = 3.6±0.2x + 2.6±0.1 and (b) calibration plots in the h-uPA concentration range 0.01-0.1 µg $mL^{-1}$ with linear fitting equation (black full line): y = 15±1x + 1.33±0.04. The values presented are the average of triplicate measurements with the associate error calculated as standard deviation.

The h-uPA concentration ranges that are clinically relevant are in the nanograms order, which means that the sensitivity of the platform must reach this level to be applied on real samples. The results reported in **Figure 31b** proved that the impedimetric platform can achieve this target both for the good linearity of the points ($R^2$>0.99) and for the LOD of 0.009 µg $mL^{-1}$, calculated by dividing the three times multiplied blank standard deviation with the slope of the linear fitting, as reported in literature,[72] which potentially makes the platform sensitive enough for clinical applications in breast cancer detection. **references such as 14-17**

# 4. Conclusions and perspectives

In this Thesis work, the synthesis, the characterization and the application of a synthetic bicyclic peptide, $P_3$, as a new bioreceptor for cancer biomarker h-uPA in a sandwich-like voltametric and impedimetric affinity assay are described.

The characterization of the biotinylated bicyclic peptide $P_3$, obtained with the automatized biotinylated resin-based SPPS synthesis of the linear peptide $P_3$ first, and upon bicyclization with TBMB then, was made with HPLC/MS analysis. From the chromatogram obtained of the sample a purity >95% was calculated and the mass spectrum revealed that the product obtained was the desired peptide.

This latter one was implemented as bioreceptor for h-uPA in a voltametric platform, in a similar fashion as already described in another case study, testing a wide concentration range (0-1 μg $mL^{-1}$). Our findings showed that the linear region of the calibration plot I vs [h-uPA] fall within 0-0.5 μg $mL^{-1}$, the same as the one described previously for another similar bicyclic peptide, $P_2$ in the same sandwich-type voltametric immunoassay.

The sensitivity of the differential pulse voltammetry-based biosensor with peptide $P_3$ was compared to that of $P_2$ and showed better performances in terms of higher slope of the calibration plot in the same linear concentration range (0-0.5 μg $mL^{-1}$): 16.0±0.9 for $P_2$, and 21.7±1.3 for $P_3$.

The synthetic biotinylated receptor $P_3$ was then used in a novel label-free impedimetric platform, whose architecture consists of a screen-printed carbon electrode functionalized with Streptavidin that can strongly immobilize $P_3$. The platform was characterized by EIS analysis, carried out on the bare electrode, the electrode functionalized with $P_3$, and the latter one upon incubation with h-uPA. When comparing the obtained EIS spectra, the growth of the Nyquist plot curves and the Bode plot peaks, which derive from the increase of resistance at the electrode surface due to the immobilized $P_3$ and h-uPA molecular layers, was verified.

From the optimization tests, where $P_3$ solutions at different concentrations (0.1 μg$mL^{-1}$, 1 μg$mL^{-1}$, 5 μg$mL^{-1}$, 10 μg$mL^{-1}$, 25 μg$mL^{-1}$ and 50 μg$mL^{-1}$) were tested using a spiked h-uPA sample (0.1 μg$mL^{-1}$), it was chosen 5 μg $mL^{-1}$ as the best choice in terms of performance and peptide economy.

Then the impedance-based assay was assessed by analyzing a wide range of h-uPA concentrations (0.01-1 μg $mL^{-1}$) and thus providing a calibration plot also for the lower concentration range (0.01-0.1 μg$mL^{-1}$), which is of high interest in diagnosis for some cancer forms, including breast cancer.

The latter calibration plot obtained showed good linearity ($R^2$ = 0.993) and a LOD (9 ng $mL^{-1}$), that allows the detection of clinical concentrations in breast cancer patients of h-uPA with this impedimetric platform.

These results confirmed that bicyclic peptides can provide an improved effectiveness as bioreceptor for many cancer biomarkers thanks also to their higher conformational stability, when compared to the linear homologues. Some of them were already proven to have high binding affinity with the marker studied in this Thesis, h-uPA. Recent research works showed that these biomolecules can be applied in analytical devices for diagnostic purposes in oncology. Moreover, they can also offer several advantages, such as portability, ease in assembling and measuring and smaller volumes used than conventional techniques.

The preliminary data obtained from the impedimetric device, described in this case study, witnessed the advantages of label-free biosensing methods and its higher sensitivity, compared to the voltammetric one.

Finding diagnostics assays that can detect nanomolar concentration of the target protein h-uPA is fundamental for the applicability of these biosensors, because of the clinical range of interest of the investigated biomarkers, in particular for breast cancer. The sensitivity showed by the two platforms in exam denotes a future possible on-field applications of these devices, although several experimental tests are yet required to verify the matrix effect due to the real samples and to validate the sensing platform in clinical settings.

# Acknowledgments

I want deeply to thank all the following people for helping and supporting me in the writing of this Thesis.

First of all, I would like to give my best thanksgivings to my supervisor, Professor Federico Polo, for his precious assistance and guidance through all this project.

I would like to thank also Professor Palchetti and Patrick Sfragano, from the University of Florence, and Prof. Cendron, from the University of Padua, for the important support in the making of the experiments.

I would like also to strongly thank Giulia, Edlind and Ylenia for supporting and helping me during all the traineeship.

I sincerely and deeply thank all my traineeship companions, Bernhard, Federica, Beatrice and Alice for all the laughs and moments together.

I want to give heartful thanks to all the people of the second floor in Epsilon for the company during lunch and coffee breaks.

I give a special thanks to all the friends that I had the pleasure to meet through my University years that stayed with me in the bad and good times.

I want to send all my deep and sincere thanks to all my high school friends, with which after more than ten years we are still closer than ever.

To all my childhood friends which are still waiting for me to start working.

To all my Bears football team teammates for all the beautiful emotions that you made and still make me feel through only one years and half.

To football, which was, is and will be my deepest passion that will accompany me for all my life.

I give all my heartful thanks to all my uncles and cousins for the beautiful family that we are.

To my grandparents, that made me live the best childhood possible, if they can hear me from up there.

To my precious family, especially my parents, for being the most patient, supporting, precious and loving people in my life.

# 5. Bibliography


1. Nenclares, P., & Harrington, K. J. (2020). The biology of cancer. *Medicine*, *48*(2), 67–72. https://doi.org/10.1016/j.mpmed.2019.11.001
2. Sung, H., Ferlay, J., Siegel, R. L., Laversanne, M., Soerjomataram, I., Jemal, A., & Bray, F. (2021). Global Cancer Statistics 2020: GLOBOCAN Estimates of Incidence and Mortality Worldwide for 36 Cancers in 185 Countries. *CA: A Cancer Journal for Clinicians*, *71*(3). https://doi.org/10.3322/caac.21660
3. Bretthauer, M., & Kalager, M. (2013). Principles, effectiveness and caveats in screening for cancer. In *British Journal of Surgery* (Vol. 100, Issue 1). https://doi.org/10.1002/bjs.8995
4. Siegel, R. L., Miller, K. D., Fuchs, H. E., & Jemal, A. (2022). Cancer statistics, 2022. *CA: A Cancer Journal for Clinicians*, *72*(1), 7–33. https://doi.org/10.3322/caac.21708
5. Parmeshwar, R., Rajan, S. S., & Shrestha, K. (2018). Principles of cancer screening. In *Surgery (United Kingdom)* (Vol. 36, Issue 3). https://doi.org/10.1016/j.mpsur.2017.12.008
6. Crippa, M. P. (2007). Urokinase-type plasminogen activator. In *International Journal of Biochemistry and Cell Biology* (Vol. 39, Issue 4). https://doi.org/10.1016/j.biocel.2006.10.008
7. Tang, L., & Han, X. (2013). The urokinase plasminogen activator system in breast cancer invasion and metastasis. In *Biomedicine and Pharmacotherapy* (Vol. 67, Issue 2). https://doi.org/10.1016/j.biopha.2012.10.003
8. Gouri, A., Dekaken, A., el Bairi, K., Aissaoui, A., Laabed, N., Chefrour, M., Ciccolini, J., Milano, G., & Benharkat, S. (2016). Plasminogen activator system and breast cancer: Potential role in therapy decision making and precision medicine. In *Biomarker Insights* (Vol. 11). https://doi.org/10.4137/Bmi.s33372
9. Mahmood, N., Mihalcioiu, C., & Rabbani, S. A. (2018). Multifaceted role of the urokinase-type plasminogen activator (uPA) and its receptor (uPAR): Diagnostic, prognostic, and therapeutic applications. In *Frontiers in Oncology* (Vol. 8, Issue FEB). https://doi.org/10.3389/fonc.2018.00024
10. Mekkawy, A. H., Pourgholami, M. H., & Morris, D. L. (2014). Involvement of Urokinase-Type Plasminogen Activator System in Cancer: An Overview. *Medicinal Research Reviews*, *34*(5). https://doi.org/10.1002/med.21308
11. Barinka, C., Parry, G., Callahan, J., Shaw, D. E., Kuo, A., Bdeir, K., Cines, D. B., Mazar, A., & Lubkowski, J. (2006). Structural Basis of Interaction between Urokinase-type Plasminogen Activator and its Receptor. *Journal of Molecular Biology*, *363*(2). https://doi.org/10.1016/j.jmb.2006.08.063
12. Duffy, M. J., O'siorain, L., O'grady, P., Devaney, D., Fennelly, J. J., & Lijnen, H. J. (1988). Urokinase-plasminogen activator, a marker for aggressive breast carcinomas. Preliminary report. *Cancer*, *62*(3). https://doi.org/10.1002/1097-0142(19880801)62:3<531::AID-CNCR2820620315>3.0.CO;2-B

**13.** Xiao, J., Zhang, G., & Xia, W. (1999). Expression and significance of urokinase-type plasminogen activator in breast cancer. *Chinese Journal of Cancer Research*, *11*(4). https://doi.org/10.1007/s11670-999-0039-2

**14.** Shiba, E., Kim, S. J., Taguchi, T., Izukura, M., Kobayashi, T., Furukawa, J., ... & Takai, S. I. (1997). A prospective study on the prognostic significance of urokinase-type plasminogen activator levels in breast cancer tissue. *Journal of cancer research and clinical oncology*, *123*, 555-559.

**15.** Borstnar, S., Vrhovec, I., Svetic, B., & Cufer, T. (2002). Prognostic value of the urokinase-type plasminogen activator, and its inhibitors and receptor in breast cancer patients. *Clinical Breast Cancer*, *3*(2). https://doi.org/10.3816/CBC.2002.n.018

**16.** Lampelj, M., Arko, D., Cas-Sikosek, N., Kavalar, R., Ravnik, M., Jezersek-Novakovic, B., Dobnik, S., Dovnik, N. F., & Takac, I. (2015). Urokinase plasminogen activator (uPA) and plasminogen activator inhibitor type-1 (PAI-1) in breast cancer-correlation with traditional prognostic factors. *Radiology and Oncology*, *49*(4). https://doi.org/10.2478/raon-2014-0049

**17.** Banys-Paluchowski, M., Witzel, I., Aktas, B., Fasching, P. A., Hartkopf, A., Janni, W., Kasimir-Bauer, S., Pantel, K., Schön, G., Rack, B., Riethdorf, S., Solomayer, E. F., Fehm, T., & Müller, V. (2019). The prognostic relevance of urokinase-type plasminogen activator (uPA) in the blood of patients with metastatic breast cancer. *Scientific Reports*, *9*(1). https://doi.org/10.1038/s41598-018-37259-2

**18.** Duffy, M. J. (2006). Urokinase-Type Plasminogen Activator and PAI-1: Validated Prognostic Factors for Breast Cancer. *Biomarkers in Breast Cancer: Molecular Diagnostics for Predicting and Monitoring Therapeutic Effect*, 111-128.

**19.** Cammann, K. (1977). Bio-sensors based on ion-selective electrodes. *Fresenius' Zeitschrift Für Analytische Chemie*, *287*(1). https://doi.org/10.1007/BF00539519

**20.** Turner, A. P. F., Karube, I., Wilson, G. S., & Worsfold, P. J. (1987). Biosensors: fundamentals and applications. *Analytica Chimica Acta*, *201*. https://doi.org/10.1016/s0003-2670(00)85361-1

**21.** Thévenot, D. R., Toth, K., Durst, R. A., & Wilson, G. S. (2001). Electrochemical biosensors: Recommended definitions and classification. *Biosensors and Bioelectronics*, *16*(1–2). https://doi.org/10.1016/S0956-5663(01)00115-4

**22.** Bergveld, P., & Thévenot, D. R. (1993). In Advances in Biosensors, Supplement 1 (APF Turner, ed.).

**23.** Cui, F., Zhou, Z., & Zhou, H. S. (2020). Review—Measurement and Analysis of Cancer Biomarkers Based on Electrochemical Biosensors. *Journal of The Electrochemical Society*, *167*(3). https://doi.org/10.1149/2.0252003jes

**24.** Singh, A., Sharma, A., Ahmed, A., Sundramoorthy, A. K., Furukawa, H., Arya, S., & Khosla, A. (2021). Recent advances in electrochemical biosensors: Applications, challenges, and future scope. In *Biosensors* (Vol. 11, Issue 9). https://doi.org/10.3390/bios11090336

**25.** Haleem, A., Javaid, M., Singh, R. P., Suman, R., & Rab, S. (2021). Biosensors applications in medical field: A brief review. In *Sensors International* (Vol. 2). https://doi.org/10.1016/j.sintl.2021.100100

**26.** Patel, P. (2017). Biosensors and Biomarkers: Promising Tools for Cancer Diagnosis. *International Journal of Biosensors & Bioelectronics*, *3*(4). https://doi.org/10.15406/ijbsbe.2017.03.00072

**27.** Sun, T., Guo, Y., & Zhao, F. (2021). Electrochemical Biosensors for the Detection of Cancer Biomarkers with Different. *International Journal of Electrochemical Science*, *16*(7). https://doi.org/10.20964/2021.07.62

**28.** Bard, A. J., Faulkner, L. R., & White, H. S. (2022). *Electrochemical methods: fundamentals and applications*. John Wiley & Sons.

**29.** Crespi, F. (2020). Differential Pulse Voltammetry: Evolution of an In Vivo Methodology and New Chemical Entries, A Short Review. *Journal of New Developments in Chemistry*, *2*(4). https://doi.org/10.14302/issn.2377-2549.jndc-20-3298

**30.** Wang, J. (2006). Controlled-Potential Techniques. In *Analytical Electrochemistry*. https://doi.org/10.1002/0471790303.ch3

**31.** Srinivasan, R., & Fasmin, F. (2021). An Introduction to Electrochemical Impedance Spectroscopy. In *An Introduction to Electrochemical Impedance Spectroscopy*. https://doi.org/10.1201/9781003127932

**32.** Magar, H. S., Hassan, R. Y. A., & Mulchandani, A. (2021). Electrochemical impedance spectroscopy (Eis): Principles, construction, and biosensing applications. In *Sensors* (Vol. 21, Issue 19). https://doi.org/10.3390/s21196578

**33.** Chang, B. Y., & Park, S. M. (2010). Electrochemical impedance spectroscopy. *Annual Review of Analytical Chemistry*, *3*(1), 207.

**34.** Taleat, Z., Khoshroo, A., & Mazloum-Ardakani, M. (2014). Screen-printed electrodes for biosensing: A review (2008-2013). In *Microchimica Acta* (Vol. 181, Issues 9–10). https://doi.org/10.1007/s00604-014-1181-1

**35.** Couto, R. A. S., Lima, J. L. F. C., & Quinaz, M. B. (2016). Recent developments, characteristics and potential applications of screen-printed electrodes in pharmaceutical and biological analysis. In *Talanta* (Vol. 146). https://doi.org/10.1016/j.talanta.2015.06.011

**36.** Moro, G., Bottari, F., van Loon, J., du Bois, E., de Wael, K., & Moretto, L. M. (2019). Disposable electrodes from waste materials and renewable sources for (bio)electroanalytical applications. In *Biosensors and Bioelectronics* (Vol. 146). https://doi.org/10.1016/j.bios.2019.111758

**37.** Cheng, W., Stuart, E. J. E., Tschulik, K., Cullen, J. T., & Compton, R. G. (2013). A disposable sticky electrode for the detection of commercial silver NPs in seawater. *Nanotechnology*, *24*(50). https://doi.org/10.1088/0957-4484/24/50/505501

**38.** Pohanka, M. (2020). Screen Printed Electrodes in Biosensors and Bioassays. A Review. *International Journal of Electrochemical Science*, *15*(11). https://doi.org/10.20964/2020.11.19

**39.** Apostolopoulos, V., Bojarska, J., Chai, T. T., Elnagdy, S., Kaczmarek, K., Matsoukas, J., New, R., Parang, K., Lopez, O. P., Parhiz, H., Perera, C. O., Pickholz, M., Remko, M., Saviano, M., Skwarczynski, M., Tang, Y., Wolf, W. M., Yoshiya, T., Zabrocki, J., … Toth, I. (2021). A global review on short peptides: Frontiers and perspectives. *Molecules*, *26*(2). https://doi.org/10.3390/molecules26020430

**40.** Nomenclature and symbolism for amino acids and peptides. (1984). *Pure and Applied Chemistry*, *56*(5). https://doi.org/10.1351/pac198456050595

**41.** Trier, N., Hansen, P., & Houen, G. (2019). Peptides, antibodies, peptide antibodies and more. In *International Journal of Molecular Sciences* (Vol. 20, Issue 24). https://doi.org/10.3390/ijms20246289

**42.** Gaspar, D., Salomé Veiga, A., & Castanho, M. A. R. B. (2013). From antimicrobial to anticancer peptides. A review. In *Frontiers in Microbiology* (Vol. 4, Issue OCT). https://doi.org/10.3389/fmicb.2013.00294

**43.** Kurrikoff, K., Aphkhazava, D., & Langel, Ü. (2019). The future of peptides in cancer treatment. In *Current Opinion in Pharmacology* (Vol. 47). https://doi.org/10.1016/j.coph.2019.01.008

**44.** Sfragano, P. S., Moro, G., Polo, F., & Palchetti, I. (2021). The role of peptides in the design of electrochemical biosensors for clinical diagnostics. In *Biosensors* (Vol. 11, Issue 8). https://doi.org/10.3390/bios11080246

**45.** Yuan, L., & Liu, L. (2021). Peptide-based electrochemical biosensing. In *Sensors and Actuators B: Chemical* (Vol. 344). https://doi.org/10.1016/j.snb.2021.130232

**46.** Gerasimov, J. Y., & Lai, R. Y. (2010). An electrochemical peptide-based biosensing platform for HIV detection. *Chemical Communications*, *46*(3). https://doi.org/10.1039/b919070h

**47.** Xia, N., Wang, X., Yu, J., Wu, Y., Cheng, S., Xing, Y., & Liu, L. (2017). Design of electrochemical biosensors with peptide probes as the receptors of targets and the inducers of gold nanoparticles assembly on electrode surface. *Sensors and Actuators, B: Chemical*, *239*. https://doi.org/10.1016/j.snb.2016.08.079

**48.** Zhao, N., He, Y., Mao, X., Sun, Y., Zhang, X., Li, C. zhong, Lin, Y., & Liu, G. (2010). Electrochemical assay of active prostate-specific antigen (PSA) using ferrocene-functionalized peptide probes. *Electrochemistry Communications*, *12*(3). https://doi.org/10.1016/j.elecom.2010.01.022

**49.** Cho, C. H., Kim, J. H., Kim, J., Yun, J. W., Park, T. J., & Park, J. P. (2021). Re-engineering of peptides with high binding affinity to develop an advanced electrochemical sensor for colon cancer diagnosis. *Analytica Chimica Acta*, *1146*. https://doi.org/10.1016/j.aca.2020.11.011

**50.** Hu, L., Hu, S., Guo, L., Shen, C., Yang, M., & Rasooly, A. (2017). DNA Generated Electric Current Biosensor. *Analytical Chemistry*, *89*(4). https://doi.org/10.1021/acs.analchem.6b04756

**51.** Koehnke, J., Naismith, J., & Van der Donk, W. A. (Eds.). (2017). *Cyclic Peptides: From Bioorganic Synthesis to Applications* (Vol. 6). Royal Society of Chemistry.

**52.** Timmerman, P., Beld, J., Puijk, W. C., & Meloen, R. H. (2005). Rapid and quantitative cyclization of multiple peptide loops onto synthetic scaffolds for structural mimicry of protein surfaces. *ChemBioChem*, *6*(5). https://doi.org/10.1002/cbic.200400374

**53.** Bozovičar, K., & Bratkovič, T. (2021). Small and simple, yet sturdy: Conformationally constrained peptides with remarkable properties. In *International Journal of Molecular Sciences* (Vol. 22, Issue 4). https://doi.org/10.3390/ijms22041611

**54.** Ali, A. M., Atmaj, J., van Oosterwijk, N., Groves, M. R., & Dömling, A. (2019). Stapled Peptides Inhibitors: A New Window for Target Drug Discovery. In *Computational and Structural Biotechnology Journal* (Vol. 17). https://doi.org/10.1016/j.csbj.2019.01.012

**55.** Robinson, J. A. (2008). β-hairpin peptidomimetics: Design, structures and biological activities. *Accounts of Chemical Research*, *41*(10). https://doi.org/10.1021/ar700259k

**56.** Rhodes, C. A., & Pei, D. (2017). Bicyclic Peptides as Next-Generation Therapeutics. In *Chemistry - A European Journal* (Vol. 23, Issue 52). https://doi.org/10.1002/chem.201702117

**57.** Diderich, P., & Heinis, C. (2014). Phage selection of bicyclic peptides binding Her2. *Tetrahedron*, *70*(42). https://doi.org/10.1016/j.tet.2014.05.106

**58.** Urech-Varenne, C., Radtke, F., & Heinis, C. (2015). Phage Selection of Bicyclic Peptide Ligands of the Notch1 Receptor. *ChemMedChem*, *10*(10). https://doi.org/10.1002/cmdc.201500261

**59.** Moreira, M., Ruggiero, A., Iaccarino, E., Barra, G., Sandomenico, A., Ruvo, M., & Berisio, R. (2021). A structure-based approach for the development of a bicyclic peptide acting as a miniaturized anti-CD55 antibody. *International Journal of Biological Macromolecules*, *182*. https://doi.org/10.1016/j.ijbiomac.2021.05.092

**60.** Blazková, K., Beranová, J., Hradilek, M., Kostka, L., Subr, V., Etrych, T., Sácha, P., & Konvalinka, J. (2021). The development of a high-affinity conformation-sensitive antibody mimetic using a biocompatible copolymer carrier (iBody). *Journal of Biological Chemistry*, *297*(5). https://doi.org/10.1016/j.jbc.2021.101342

**61.** Timmerman, P., Barderas, R., Desmet, J., Altschuh, D., Schochat, S., Hollestelle, M. J., Höppener, J. W. M., Monasterio, A., Casal, J. I., & Meloen, R. H. (2009). A Combinatorial approach for the design of complementarity-determining region-derived peptidomimetics with in vitro anti-tumoral activity. *Journal of Biological Chemistry*, *284*(49). https://doi.org/10.1074/jbc.M109.041459

**62.** Watson, G. M., Kulkarni, K., Sang, J., Ma, X., Gunzburg, M. J., Perlmutter, P., Wilce, M. C. J., & Wilce, J. A. (2017). Discovery, Development, and Cellular Delivery of Potent and Selective Bicyclic Peptide Inhibitors of Grb7 Cancer Target. *Journal of Medicinal Chemistry*, *60*(22). https://doi.org/10.1021/acs.jmedchem.7b01320

**63.** Roodbeen, R., Paaske, B., Jiang, L., Jensen, J. K., Christensen, A., Nielsen, J. T., Huang, M., Mulder, F. A. A., Nielsen, N. C., Andreasen, P. A., & Jensen, K. J. (2013). Bicyclic peptide inhibitor of urokinase-type plasminogen activator: Mode of action. *ChemBioChem*, *14*(16). https://doi.org/10.1002/cbic.201300335

**64.** Hansen, M., Wind, T., Blouse, G. E., Christensen, A., Petersen, H. H., Kjelgaard, S., Mathiasen, L., Holtet, T. L., & Andreasen, P. A. (2005). A urokinase-type plasminogen activator-inhibiting cyclic peptide with an unusual P2 residue and an extended protease binding surface demonstrates new modalities for enzyme inhibition. *Journal of Biological Chemistry*, *280*(46). https://doi.org/10.1074/jbc.M505933200

**65.** Henneke, I., Greschus, S., Savai, R., Korfei, M., Markart, P., Mahavadi, P., Schermuly, R. T., Wygrecka, M., Stürzebecher, J., Seeger, W., Günther, A., & Ruppert, C. (2010). Inhibition of urokinase activity reduces primary tumor growth and metastasis formation in a murine lung carcinoma model. *American Journal of Respiratory and Critical Care Medicine*, *181*(6). https://doi.org/10.1164/rccm.200903-0342OC

**66.** Angelini, A., Cendron, L., Chen, S., Touati, J., Winter, G., Zanotti, G., & Heinis, C. (2012). Bicyclic peptide inhibitor reveals large contact interface with a protease target. *ACS Chemical Biology*, *7*(5). https://doi.org/10.1021/cb200478t

**67.** Moro, G., Sfragano, P. S., Ghirardo, J., Mazzocato, Y., Angelini, A., Palchetti, I., & Polo, F. (2022). Bicyclic peptide-based assay for uPA cancer biomarker. *Biosensors and Bioelectronics*, *213*, 114477.

**68.** Moro, G., Bottari, F., Liberi, S., Covaceuszach, S., Cassetta, A., Angelini, A., de Wael, K., & Moretto, L. M. (2020). Covalent immobilization of delipidated human serum albumin on poly(pyrrole-2-carboxylic) acid film for the impedimetric detection of perfluorooctanoic acid. *Bioelectrochemistry*, *134*. https://doi.org/10.1016/j.bioelechem.2020.107540

**69.** Mazzocato, Y., Frasson, N., Angelini, A. (2022). Inibitori peptidici biciclici dell'attivatore del plasminogeno di tipo urochinasi umana (huPA). https://hdl.handle.net/10278/5007900

**70.** Daems, E., Moro, G., Campos, R., & de Wael, K. (2021). Mapping the gaps in chemical analysis for the characterisation of aptamer-target interactions. In *TrAC - Trends in Analytical Chemistry* (Vol. 142). https://doi.org/10.1016/j.trac.2021.116311

**71.** Pinkova Gajdosova, V., Lorencova, L., Blsakova, A., Kasak, P., Bertok, T., & Tkac, J. (2021). Challenges for impedimetric affinity sensors targeting protein detection. In *Current Opinion in Electrochemistry* (Vol. 28). https://doi.org/10.1016/j.coelec.2021.100717

**72.** Solis-Marcano, N. E., Morales-Cruz, M., Vega-Hernández, G., Gómez-Moreno, R., Binder, C., Baerga-Ortiz, A., Priest, C., & Cabrera, C. R. (2021). PCR-assisted impedimetric biosensor for colibactin-encoding pks genomic island detection in E. coli samples. *Analytical and Bioanalytical Chemistry*, *413*(18). https://doi.org/10.1007/s00216-021-03404-6